Sensitivities of the Lower-Stratospheric Transport and Mixing to Tropical SST Heating

HUANG YANG AND GANG CHEN

Department of Earth and Atmospheric Sciences, Cornell University, Ithaca, New York

DANIELA I. V. DOMEISEN

Institute of Oceanography, University of Hamburg, Hamburg, Germany

(Manuscript received 3 September 2013, in final form 31 January 2014)

ABSTRACT

The sensitivities of the Brewer–Dobson circulation (BDC) to different distributions of tropical SST heating are investigated in an idealized aquaplanet model. It is found that an increase in tropical SSTs generally leads to an acceleration of tropical upwelling and an associated reduction in the age of air (AOA) in the polar stratosphere and that the AOA near the subtropical tropopause is correlated with local isentropic mixing of tropospheric air with stratospheric air.

The zonal distribution of SST perturbations has a major impact on the vertical and meridional structure of the BDC as compared with other SST characteristics. Zonally localized SST heatings tend to generate a shallow acceleration of the stratospheric residual circulation, enhanced isentropic mixing associated with a weakened stratospheric jet, and a reduction in AOA mostly within the polar vortex. In contrast, SST heatings with a zonally symmetric structure tend to produce a deep strengthening of the stratospheric residual circulation, suppressed isentropic mixing associated with a stronger stratospheric jet, and a decrease of AOA in the entire stratosphere. The shallow versus deep strengthening of the stratospheric residual circulation change has been linked to wave propagation and dissipation in the subtropical lower stratosphere rather than wave generation in the troposphere, and the former can be strongly affected by the vertical position of the subtropical jet. These results suggest that, while the longitudinally localized SST trends under climate change may contribute to the change in the shallow branch of the BDC, the upward shift of the subtropical jet associated with the zonal SST heating can impact the deep branch of the BDC.

1. Introduction

The Brewer–Dobson circulation (BDC; Brewer 1949; Dobson 1956) is important for the dynamics and distribution of chemical constituents in the stratosphere, and consequently impacts stratospheric chemistry and climate. In the lower stratosphere, the upwelling across the tropical tropopause acts as a primary path for troposphere-to-stratosphere mass transport, and the isentropic mixing across the subtropical and extratropical tropopause provides a two-way exchange of air masses through blocking anticyclones, cutoff cyclones, or tropopause folds (e.g., Holton et al. 1995).

It is well known that tropical sea surface temperature (SST) can impact the lower stratospheric transport. The latent heat released from deep convection can induce an upwelling across the tropical tropopause layer (TTL) by local wave drag (Norton 2006; Ryu and Lee 2010), and this has been used to explain the seasonal cycle of the tropical upwelling (Kerr-Munslow and Norton 2006; Deckert and Dameris 2008). During the warm phase of the El Niño–Southern Oscillation (ENSO) cycle, the isentropic mixing near the tropopause is found to be weaker than normal (Scott and Cammas 2002; Scott et al. 2003), but the mean residual meridional circulation is intensified in the lower tropical troposphere (Calvo et al. 2010; Simpson et al. 2011), with a negative correlation between tropical Pacific SSTs and temperature in the tropical lower stratosphere (Hardiman et al. 2007; Calvo et al. 2010). Furthermore, under greenhouse gas warming, chemistry–climate models (CCMs) predict a consistent acceleration of the residual circulation in

Corresponding author address: Huang Yang, 1126 Bradfield Hall, Department of Earth and Atmospheric Sciences, Cornell University, Ithaca, NY 14853.
E-mail: hy337@cornell.edu

DOI: 10.1175/JAS-D-13-0276.1

the tropical lower stratosphere and a reduction in the age of stratospheric air (e.g., Li et al. 2008; Garcia and Randel 2008; McLandress and Shepherd 2009; Butchart et al. 2010; Garny et al. 2011), accompanied with more stratosphere-to-troposphere ozone transport in the extratropics (e.g., Hegglin and Shepherd 2009). The increase in tropical upwelling is consistent with radiosonde observations with a cooling trend of tropical tropopause temperature (Thompson and Solomon 2005) and this effect of greenhouse gas warming has been primarily attributed to tropical SST heating (Garny et al. 2011). However, it is difficult to detect this trend in the age of stratospheric air from balloon-borne measurements of stratospheric trace gases (Engel et al. 2008), since the mean age trends estimated from the observations can have large uncertainties due to sparse spatial sampling (Ray et al. 2010; Garcia et al. 2011). It is then important to understand how the SST variability impacts different diagnostics of stratospheric transport circulations.

The mean isentropic circulation, often approximated by the transformed Eulerian mean (TEM) residual circulation (Andrews et al. 1987), generally rises in the deep tropics and descends at middle and high latitudes. The strength of the tropical upwelling can be derived from either resolved or parameterized wave drag through the well-known downward control mechanism (Haynes et al. 1991; Holton et al. 1995), which provides a framework to attribute the tropical upwelling to individual wave forcings. The increased tropical upwelling during El Niño has been linked to Northern Hemisphere (NH) planetary waves (García-Herrera et al. 2006), orographic gravity wave drag in the NH (Calvo et al. 2010), or the transient synoptic-scale wave drag in the Southern Hemisphere (SH) (Simpson et al. 2011). The acceleration of the BDC under climate change has been attributed to the individual contributions from the resolved planetary-scale waves, synoptic-scale waves, or parameterized gravity waves, and different forcing mechanisms are found to be equally important for the trend in the BDC (McLandress and Shepherd 2009). More specifically, the increased planetary wave drag has been explained as a consequence of changes in the propagation characteristics in the stratosphere (e.g., Rind et al. 1998; Olsen et al. 2007), increased wave generation in the lower troposphere (Eichelberger and Hartmann 2005), or increased wave flux from the troposphere into the stratosphere (Garcia and Randel 2008; McLandress and Shepherd 2009). Recently, Shepherd and McLandress (2011) argued that these changes in resolved wave drag can be explained by a critical layer control of the subtropical wave breaking, which in turn can be attributed to the strengthened upper flank of the subtropical jet associated with robust tropical warming and stratospheric cooling.

Another important, albeit less studied, ingredient of the BDC is isentropic mixing. For long-lived constituents in the stratosphere, their equilibrium distributions are controlled by a balance between a slow overturning circulation and rapid mixing along isentropic surfaces (e.g., Holton 1986; Mahlman et al. 1986). Plumb (2002) showed with a scale analysis that the isentropic stirring dominates the tracer budget within the surf zone over the mean isentropic transport. Using the concept of effective diffusivity (Nakamura 1996), it is found that isentropic mixing is characterized by enhanced mixing within the surf zone and mixing barriers in the subtropics and at the polar vortex edge (Haynes and Shuckburgh 2000a,b; Allen and Nakamura 2001), and that the locations of enhanced (weakened) isentropic mixing coincide with the regions of weak (strong) zonal winds. Furthermore, Shuckburgh et al. (2009) showed that ENSO modulates the Lyapunov diffusivity across the subtropical jet in agreement with the results in Scott et al. (2003) with effective diffusivity.

In this study, we will investigate the connection between the tropical SST variability and the BDC. Given the uncertainties of the tropical circulation to model physical parameterizations, we employ an idealized aquaplanet model with simple SST profiles. While the simplicity of the model does not allow for a direct comparison to observations (as discussed in section 2c, the idealized model does not include stationary planetary waves in the control run), it allows for a systematic investigation of the mechanisms that link tropical SST variability and transport changes in the lower stratosphere.

It is noteworthy that while El Niño and global warming are both characterized by warming in the tropical upper troposphere, the latitudinal changes in the jet streams are opposite in sign (e.g., Lu et al. 2008; Chen et al. 2008, 2010), which may result in different characteristics in tropospheric wave generation and propagation. We vary both the zonal distribution and the meridional width of the SST perturbations. We found that the key to the response in the stratospheric transport is the zonal distribution of the SST heating: a longitudinally localized heating drives a shallow acceleration of the BDC, but a zonally symmetric heating intensifies the BDC up to a higher altitude associated with an upward-shifted subtropical jet. The different responses can be attributed to the combined effects of tropical heating on the lower stratospheric zonal wind versus the convection-induced planetary waves.

The model and methods applied in this study are briefly described in section 2. In section 3, we will compare the BDC responses to longitudinally localized versus zonally

symmetric tropical heating and the responses to meridionally narrow versus broad tropical heating, with a highlight on the changes in the residual circulation, isentropic mixing, and AOA. Section 4 further examines the sensitivities of the lower-stratospheric transport to the zonal asymmetry of tropical SST heating. Section 5 explores the mechanisms behind the changes in the residual circulation and isentropic mixing. A summary and discussion are given in section 6.

2. Aquaplanet model and transport diagnostics

a. The aquaplanet model and experiment setup

We use the aquaplanet version of the Geophysical Fluid Dynamics Laboratory (GFDL) atmospheric model, AM2.1 (Delworth et al. 2006), but with increased stratospheric resolution. The model is run at a horizontal resolution of approximately 2.5° (longitude) by 2° (latitude), and the standard 24 vertical levels of AM2.1 are increased to 48 levels with the top close to 0.01 hPa, following the vertical levels of AM3 (Donner et al. 2011). There is no subgrid parameterization for orographic or convective gravity waves. At the top of the model, the linear drag at the top layer in AM2.1 has been replaced by a simple sponge layer described in Polvani and Kushner (2002), with a linear damping increasing gradually from 0.5 hPa to the model top.

The model physics package follows the specifications in the Aqua-Planet Experiment (APE) project described in Neale and Hoskins (2000). The solar radiative forcing is fixed in the equinoctial condition but the diurnal cycle is included. The ozone mixing ratio is prescribed as the annual mean climatology used in the Atmospheric Model Intercomparison Project (AMIP) II. Other radiatively active gases such as CO_2 are well mixed and their mixing ratios adopt the AMIP II recommendations and there are no radiatively active aerosols. There is no topography at the surface, and an idealized SST profile is specified with no sea ice. In the control simulation, the SST is specified as the Qobs profile described in Neale and Hoskins (2000):

$$T_{\text{ctrl}} = 27 \times (0.5 \sin^2\phi' + \sin^4\phi'), \tag{1}$$

where $\phi' = \max[\min(3\phi/2, \pi/2), -(\pi/2)]$ and ϕ denotes latitude. The SST profile can be thought of as the annual and zonal mean SST in the observations (contours in Fig. 1). In this simple setting, there are no stationary waves in the model but transient planetary waves exist.

We investigate the impact of tropical SST perturbations on the BDC. The control SST profile, Eq. (1), is perturbed by

$$T_{\text{anmly}} = A_0 \times \exp\left[-\left(\frac{\lambda-\lambda_0}{\lambda_S}\right)^2 - \left(\frac{\phi-\phi_0}{\phi_S}\right)^2\right], \tag{2}$$

where the SST anomaly has a peak of amplitude $A_0 = 3$ K centered at the longitude $\lambda_0 = 180°$ and the equator $\phi_0 = 0°$. Our primary foci are the parameters for the meridional width of the tropical SST perturbation ϕ_S and its zonal asymmetry given by λ_S. We start by comparing the circulation responses to the four SST anomalies illustrated in Fig. 1 with varied zonal asymmetry and meridional width:

- LATnLONn heating: latitudinally narrow with $\phi_S = 15°$, longitudinally narrow with $\lambda_S = 30°$,
- LATnLONs heating: latitudinally narrow with $\phi_S = 15°$, longitudinally symmetric with $\lambda_S = \infty$,
- LATbLONn heating: latitudinally broad with $\phi_S = 30°$, longitudinally narrow with $\lambda_S = 30°$,
- LATbLONs heating: latitudinally broad with $\phi_S = 30°$, longitudinally symmetric with $\lambda_S = \infty$.

It will be demonstrated that the zonal distribution of tropical heating has a stronger effect on the lower stratospheric transport although the meridional width of the heating has a stronger effect on the tropospheric jet latitude. To further illustrate the effect of the zonal SST distribution, the longitudinal extent of the SST perturbation λ_S is varied using values of 15°, 30°, 60°, 90°, 150°, and ∞. The monotonic increase of λ_S allows for a change in the longitudinal extent of the SST perturbation from a longitudinally narrow heating ($\lambda_S = 15°$) to a zonally symmetric setup ($\lambda_S = \infty$). Additionally, we have also varied the latitude of maximum heating ϕ_0 and the amplitude of SST heating A_0. The results are qualitatively similar and are reported briefly in section 4a. All integrations are run for 14 years, with the first-year spinup data discarded. As we are mostly interested in dynamically consistent patterns, we choose to focus on the dominant features of the circulation response. Our results can be reproduced by half of the time series, confirming the statistical significance of our results. The data are sampled instantaneously at a frequency of four times daily for the diagnostics of eddy fluxes and isentropic mixing.

b. Diagnostic methods

Transport and mixing in the stratosphere are diagnosed using three metrics: 1) the residual mean meridional circulation that approximates the mean diabatic circulation, 2) the equivalent lengths of potential vorticity (PV) contours that describe the isentropic eddy mixing, and 3) the mean age of air (AOA) in the stratosphere.

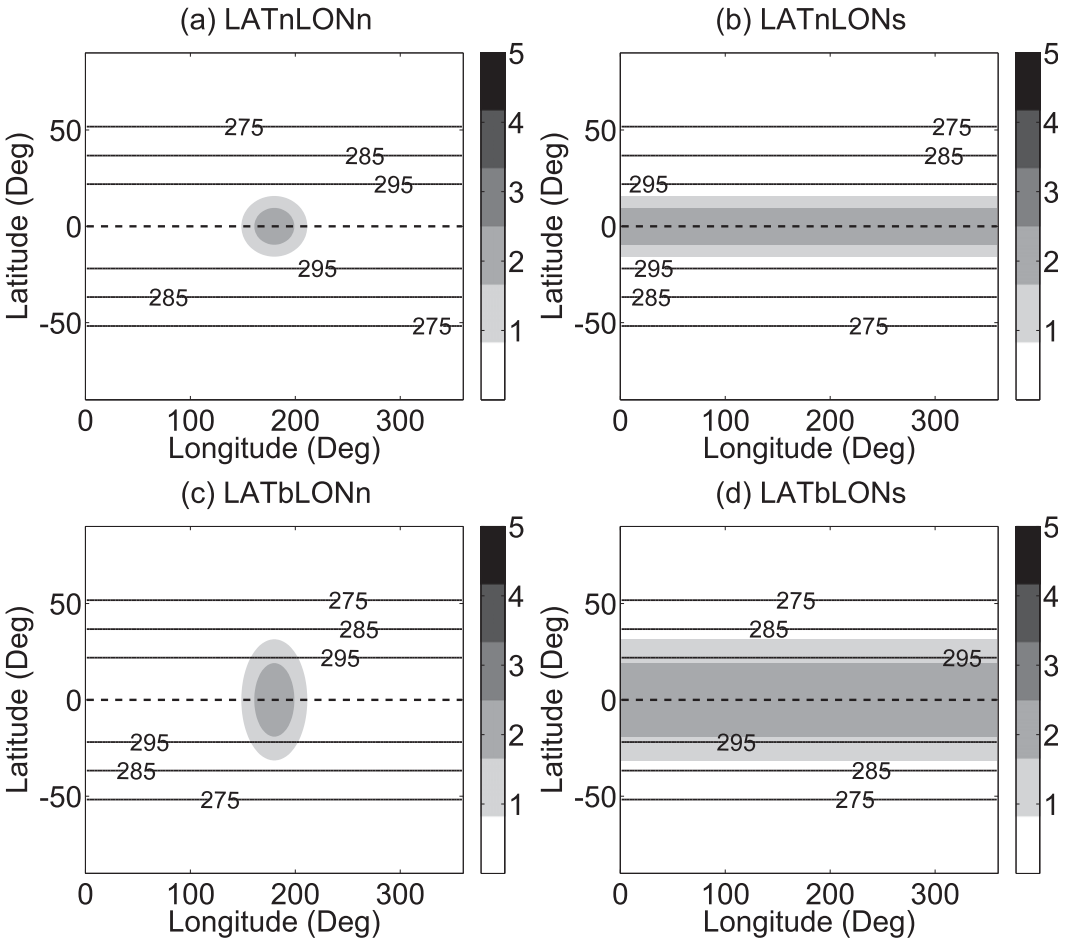

FIG. 1. Prescribed SST forcing (K): the control run is shown by the solid contours and the SST perturbations are depicted by the shading. (a) Latitudinally narrow and longitudinally narrow (LATnLONn) heating ($\phi_S = 15°, \lambda_S = 30°$); (b) latitudinally narrow and longitudinally symmetric (LATnLONs) heating ($\phi_S = 15°, \lambda_S = \infty$); (c) latitudinally broad and longitudinally narrow (LATbLONn) heating ($\phi_S = 30°, \lambda_S = 30°$); and (d) latitudinally broad and longitudinally symmetric (LATbLONs) heating ($\phi_S = 30°, \lambda_S = \infty$). The equator is marked by the dashed line.

1) RESIDUAL MERIDIONAL MEAN CIRCULATION

In the limit of quasigeostrophic scaling, the mean diabatic circulation in the stratosphere can be approximated by the transformed Eulerian mean circulation in geometric coordinates (Edmon et al. 1980; Andrews et al. 1987). More specifically, the residual vertical velocity can be written as

$$\overline{w}^* = \overline{w} - \frac{1}{\rho_0 g a \cos\phi}\frac{\partial}{\partial\phi}\left(\cos\phi\frac{\overline{v'\theta'}}{\overline{\theta}_p}\right). \qquad (3)$$

Here ϕ, p, g, a, ρ_0, and θ denote latitude, pressure, gravitational acceleration, radius of Earth, zonal mean density, and potential temperature, respectively; $\overline{w}$ is the conventional Eulerian mean (zonal mean) vertical velocity and $\overline{v'\theta'}$ represents the eddy heat flux.

The residual circulation can be diagnosed from the resolved or parameterized wave drag through the ''downward control'' principle in the TEM equations (Haynes et al. 1991). From the momentum balance, the residual vertical velocity averaged between the latitudes ϕ_1 and ϕ_2 can be calculated from the integral of the resolved wave drag DF above the layer of interest:

$$\langle\overline{w}^*_m\rangle(p) = \frac{1}{\rho_0(p)g\int_{\phi_1}^{\phi_2} a\cos\phi\,\mathrm{d}\phi} \times\left\{-\cos\phi\int_0^p \frac{[\mathrm{DF}(\phi,p') - \overline{X}]}{\hat{f}(\phi,p')}\mathrm{d}p'\right\}_{\phi_1}^{\phi_2}, \qquad (4)$$

where $\langle\rangle$ denotes the latitudinal average, and $\overline{X}$ denotes the parameterized wave drag in the model. The modified Coriolis parameter is given by $\hat{f} = f - (1/a\cos\phi)(\partial/\partial\phi)(\overline{u}\cos\phi)$. The curly brackets denote a subtraction of the quantity inside the bracket at the latitude ϕ_2 by its value at the latitude ϕ_1. We set $\phi_1 = -15°$ and $\phi_2 = 15°$ over the deep tropics following Randel et al. (2008). This latitudinal average avoids the singularity of the Coriolis parameter near the equator and facilitates the calculation of the averaged vertical velocity from the meridional mass flux across the northern and southern boundaries. The resolved wave drag DF is given by the Eliassen–Palm (EP) flux divergence:

$$\mathrm{DF} = \frac{1}{a\cos\phi}\nabla\cdot\mathbf{F} = \frac{1}{a\cos\phi}\left[\frac{1}{a\cos\phi}\frac{\partial(F_\phi\cos\phi)}{\partial\phi} + \frac{\partial F_p}{\partial p}\right], \tag{5}$$

where $\mathbf{F}$ is the EP flux vector with components

$$F_\phi = a\cos\phi\left[-\overline{v'u'} + \left(\frac{\partial\overline{u}}{\partial p}\right)\frac{\overline{v'\theta'}}{\overline{\theta}_p}\right] \quad \text{and} \tag{6a}$$

$$F_p = a\cos\phi\left[\hat{f}\frac{\overline{v'\theta'}}{\overline{\theta}_p} + \rho_0 g\overline{w'u'}\right]. \tag{6b}$$

Furthermore, the residual vertical velocity can also be diagnosed from the thermodynamic balance with the diabatic heating $\overline{Q}$:

$$\overline{w}^*_Q = -\frac{1}{\rho_0 g}\frac{\overline{Q}(\theta,p)}{\overline{\theta}_p}. \tag{7}$$

The comparison between $\overline{w}^*$ and $\overline{w^*_m}$ determines to what extent the tropical upwelling is wave driven, and the consistency between $\overline{w}^*$ and $\overline{w}^*_Q$ indicates the adjustment in diabatic heating approximately balances the wave-driven circulation.

2) Isentropic mixing

Tracers in the stratosphere are subject to rapid eddy mixing along isentropic surfaces. For a passive tracer that varies monotonically with latitude, we can characterize the isentropic mixing by the "equivalent length" of tracer contours (Nakamura 1996; Haynes and Shuckburgh 2000a; Allen and Nakamura 2001), given by

$$L_e^2 = \frac{\partial}{\partial A}\iint_{A(q,t)}|\nabla q|^2\,dA\Big/\left(\frac{\partial q}{\partial A}\right)^2, \tag{8}$$

where q is the mixing ratio of a passive tracer, and A is the area bounded by the tracer contour q around the North Pole. The area A is defined by an equivalent latitude ϕ_e by $A = 2\pi a^2(1 - \sin\phi_e)$. In regions of strong mixing along isentropic surfaces, the tracer contours are expected to be long and complex in geometry. The equivalent length is greater than or equal to the actual length of tracer contours (Haynes and Shuckburgh 2000a). If the tracer contour exactly follows a latitude circle, its equivalent length shrinks to its minimum value (i.e., the length $2\pi a\cos\phi_e$ of that latitude circle for a given latitude ϕ_e). Thus, the equivalent length ratio $\tilde{\kappa}_{\mathrm{eff}} = L_e^2/(2\pi a\cos\phi_e)^2$ provides a nondimensional measure of the strength of isentropic eddy mixing. If the diffusion coefficient [κ in Eq. (3) of Haynes and Shuckburgh 2000a] is a constant, $\tilde{\kappa}_{\mathrm{eff}}$ is proportional to the effective diffusivity in isentropic mixing that is defined by the mass flux across the tracer contours (Nakamura 1996). More generally, if the exact form of small-scale diffusion is not known, the equivalent length can still describe the degree of eddy mixing as the effective diffusivity is dictated by the large-scale stirring and stretching (Allen and Nakamura 2001).

The tracer in the equivalent length calculation can either be a dynamical tracer such as Ertel's PV or a long-lived chemical tracer in the stratosphere such as SF_6. Haynes and Shuckburgh (2000a) also calculated the equivalent length of a passive tracer advected by the isentropic winds, which is consistent with the mixing length of the PV. In this study, we will calculate the equivalent length using Ertel's PV, $q = -g\zeta_a(\partial\theta/\partial p)$, where ζ_a is the absolute vorticity on an isentropic surface.

3) Age of air

Another diagnostic of stratospheric transport is the mean age of stratospheric air, the transit time from the tropical tropopause to a location within the stratosphere (e.g., Hall and Plumb 1994; Waugh and Hall 2002). In this diagnostic, a clock tracer is specified to grow linearly in time in the source region below 750 hPa, and above this level the tracer is conservative except for small-scale diffusion. For a tracer concentration growing linearly at its source, the mixing ratio of the tracer elsewhere is expected to increase linearly with the same growth rate but reaches a certain magnitude later than at the source (see Fig. 1 in Waugh 2009). This time lag defines the mean AOA, given by

$$\Gamma = t(\chi;\phi,p) - t(\chi;\phi_0,p_0), \tag{9}$$

where χ is the mixing ratio of the tracer, and ϕ_0 and p_0 denote the latitude and pressure of the reference point. The mean AOA can be influenced by both mean isentropic

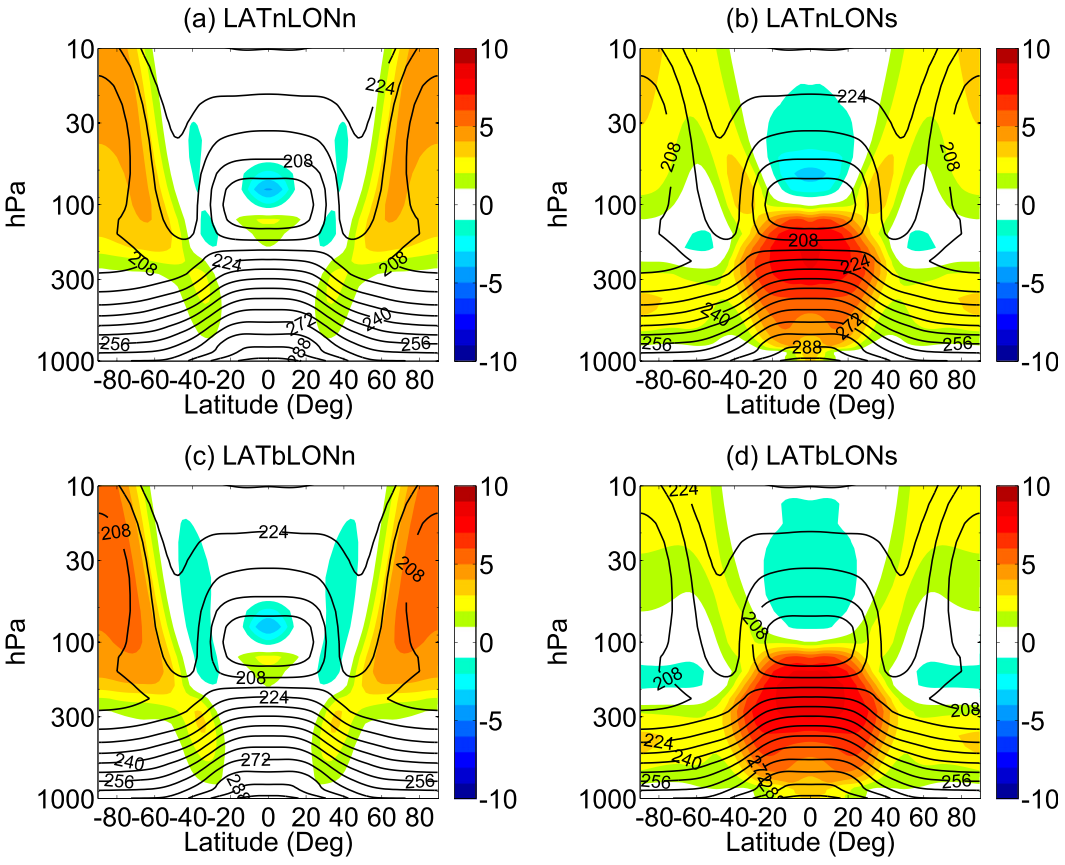

FIG. 2. Climatology of the control run (K; contours) and the change in zonal mean temperature (K; shading) for (a) LATnLONn, (b) LATnLONs, (c) LATbLONn, and (d) LATbLONs.

circulation and eddy mixing. For the age of stratospheric air, the reference point is generally chosen at the tropical tropopause. We follow Garcia et al. (2011) by calculating the mean AOA using the monthly averaged mixing ratio of the age tracer, and setting the reference point at $\phi_0 = 0$, $p_0 = 150$ hPa.

c. *Atmospheric circulation in the control simulation*

The control simulation can approximately reproduce the basic features of the observed annual mean atmospheric circulation and transport, also shown in the contours of Figs. 2–5. The dome-shaped tropopause and the tropical "cold point" aloft are both captured in this simulation (Fig. 2), as well as the tropospheric subtropical jets and stratospheric jets (Fig. 3). However, because of the absence of stationary planetary waves in this simulation, the zonal mean zonal winds are stronger in magnitude than those in observations, particularly in the NH stratosphere where stationary planetary waves exert a strong wave drag on the stratospheric winter circulation. We therefore focus on the annual mean responses in this study, rather than the winter season that most other studies concentrate on when exploring the stratosphere–troposphere coupling and transport. Similarly, the transient planetary waves and synoptic-scale waves in the model can simulate a reasonable magnitude of the residual circulation in the troposphere and lower stratosphere, whereas the residual circulation in the middle and upper stratosphere is weaker than the observed circulation due to a lack of stationary planetary waves (Fig. 4). As a result, the model can simulate a reasonable structure in AOA (Fig. 5), although the air in the upper stratosphere is older than in observations. In the next section, we will compare these climatological patterns with the SST-forced changes shown in color.

As for isentropic mixing, Fig. 6 shows the climatological mean isentropic eddy mixing and EP flux divergence in the control run. The equivalent length is calculated on each isentropic surface, and the time mean equivalent length is interpolated linearly to pressure surfaces. As found in observations (Haynes and Shuckburgh 2000b), the intensity of isentropic eddy mixing is roughly anticorrelated with the strength of the zonal mean zonal wind. Mixing maxima occur in the stratospheric surf

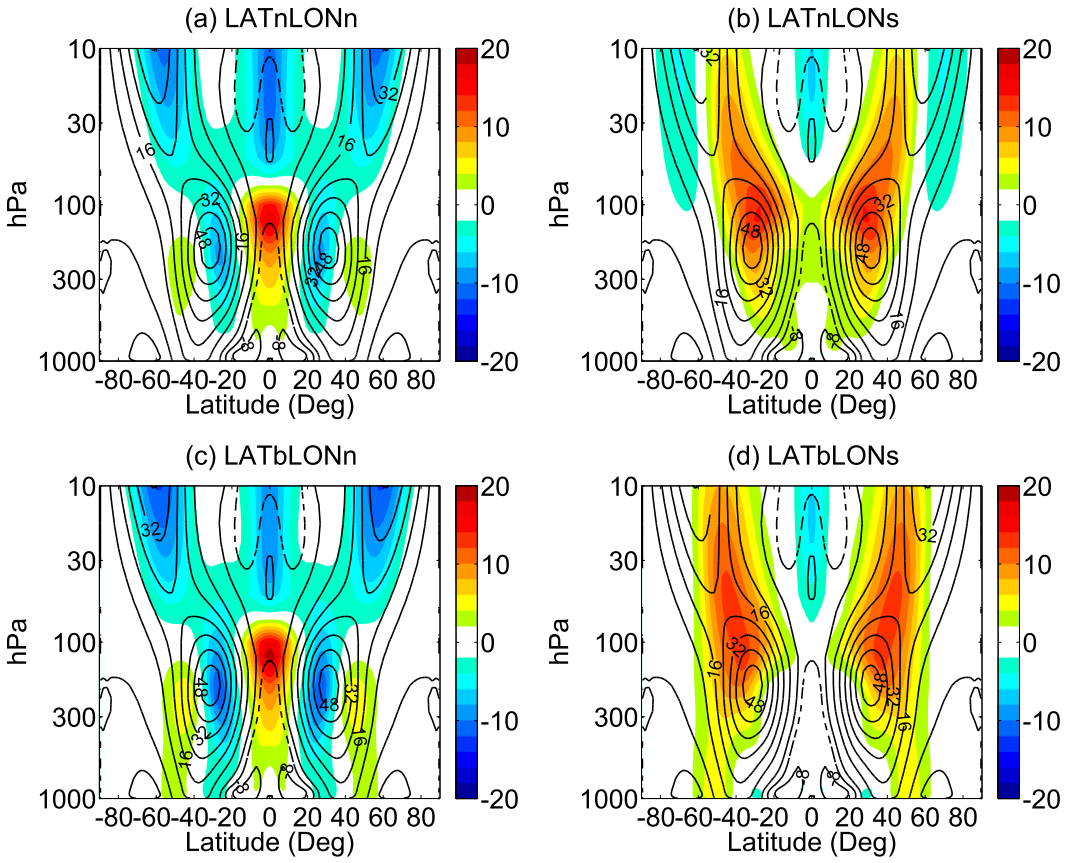

FIG. 3. As in Fig. 2, but for the zonal mean zonal wind ($m\,s^{-1}$; solid contours for positive, dashed contours for negative).

zone and at the flanks of the tropospheric jets where the zonal winds are weak. Isentropic mixing is suppressed at the stratospheric jet and subtropical jet with prevailing westerlies, and the weak mixing results in transport barriers that lead to a large latitudinal gradient in mean AOA (not shown here). Furthermore, the regions of strong eddy mixing are also roughly consistent with the regions of large EP flux convergence where wave breaking is frequent. Baroclinic synoptic-scale eddies are generated within the extratropical lower troposphere and are mostly dissipated in the extratropical middle and upper troposphere. Even in the absence of topographical forcing, transient planetary waves can be generated through eddy–eddy interactions (Scinocca and Haynes 1998). These planetary-scale waves are allowed to propagate vertically into the stratosphere, and the subsequent breaking of stratospheric waves results in rapid mixing of air masses along isentropic surfaces.

Conventionally, research has focused on the winter hemisphere when discussing stratosphere–troposphere coupling and transport (e.g., Gerber 2012). Here, our simulations correspond to the annual mean condition for simplicity. Without topography and land–sea contrast, the simulated polar vortex in the stratosphere will be unrealistically strong if the aquaplanet model adopts a solstitial condition. Therefore, the current setting of the control simulation is more suitable for the problem we are investigating. As the result of the simplicity of the aquaplanet model, we will not examine the effects of gravity waves or orographic Rossby waves. However, similarities of the residual circulation response are still found by comparing the results from our idealized simulation (see details in section 3) with the ones in a comprehensive model where these waves are resolved or parameterized (Garny et al. 2011).

3. BDC responses to different zonal and latitudinal distributions of tropical SST heating

We begin to investigate the patterns of tropical SST-forced stratospheric transport changes using four types of tropical heating as illustrated in Fig. 1. Specifically, we compare longitudinally narrow ($\lambda_S = 30°$, denoted by LONn) heating (Fig. 1, left column) with longitudinally

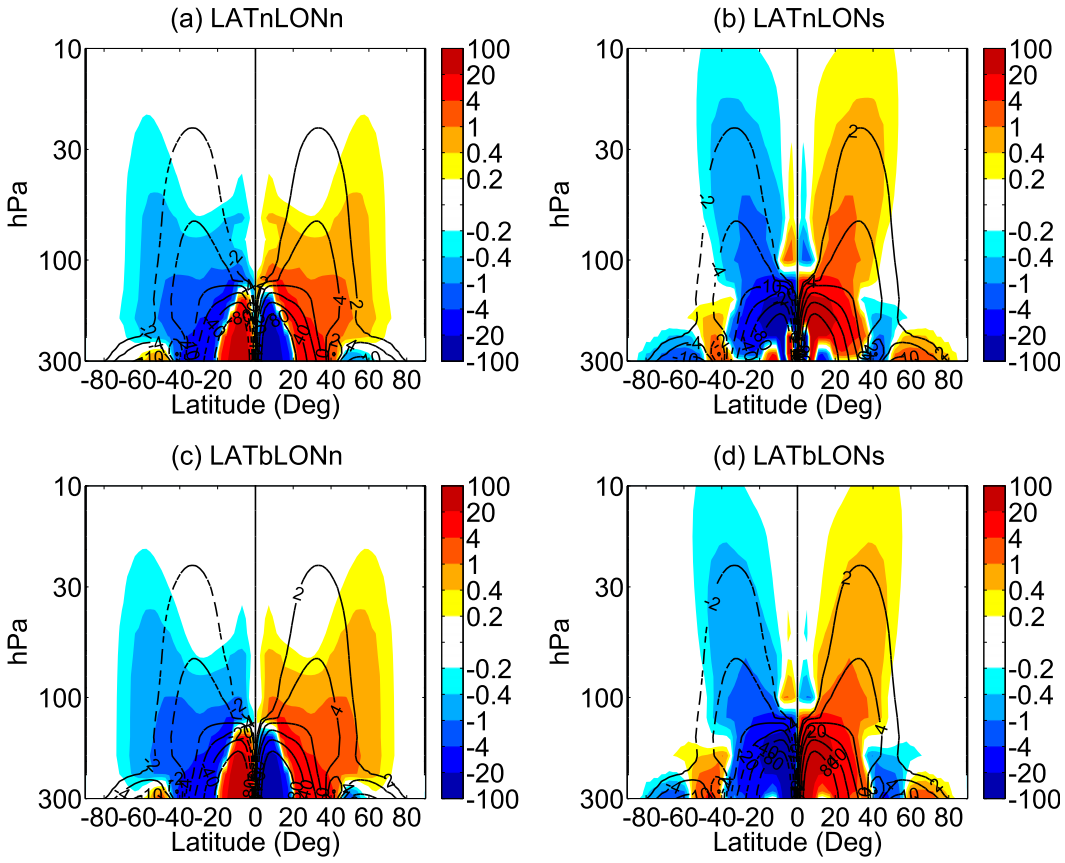

FIG. 4. As in Fig. 3, but for the residual streamfunction $\overline{\chi}^*$ (10^9 kg s^{-1}). Warm shading and solid contours depict anticyclonic circulation whereas cold shading and dashed contours depict cyclonic circulation. Note that the vertical axis has been changed to 10–300 hPa.

symmetric ($\lambda_S = \infty$, denoted by LONs) heating (Fig. 1, right column). For both LONn and LONs, we also compare latitudinally narrow ($\phi_S = 15°$, denoted by LATn) heating (Fig. 1, top row) with latitudinally broad ($\lambda_S = 30°$, denoted by LATb) heating (Fig. 1, bottom row). The changes in atmospheric circulation and transport are presented in the same fashion.

Figure 2 displays the changes in zonal mean temperature (shading) in each simulation with respect to the climatology of the control run (contours). All tropical heating patterns lead to warming in the tropical upper troposphere, cooling in the tropical lower stratosphere, and warming in the polar stratosphere. This spatial pattern is qualitatively consistent with the temperature response associated with the ENSO cycle (e.g., Randel et al. 2009) and with the tropical SST heating due to greenhouse gases (Garny et al. 2011). The warming over the stratospheric polar caps in the experiments with LONn heating (left column) is larger than that with LONs heating (right column). The tropospheric warming, on the other hand, is pronounced only in the tropical upper troposphere and subtropics for LONn heating, while the warming is spread over the entire tropics for LONs heating.

As for zonal mean zonal wind (Fig. 3), for LONn heating (left column), the easterlies in the deep tropics are weakened and even transition to westerlies. With the biggest eastward acceleration at approximately 150 hPa, superrotation develops through equatorial deep convection as found in Liu and Schneider (2011). The tropospheric subtropical jet is decelerated on its equatorward flank, and the jet in the stratosphere is weakened. By contrast, for LONs heating (right column) the tropospheric subtropical jet is shifted upward, and the zonal mean zonal wind is increased on the equatorward flank of the stratospheric jet. With less deceleration about the stratospheric jet for LONs heating, less warming is observed over the stratospheric polar caps as compared to LONn heating. This suggests a smaller wave drag in the (lower) stratosphere given a zonally symmetric heating in the LONs runs. Moreover, for the two LONs experiments, the subtropical jet moves equatorward for the

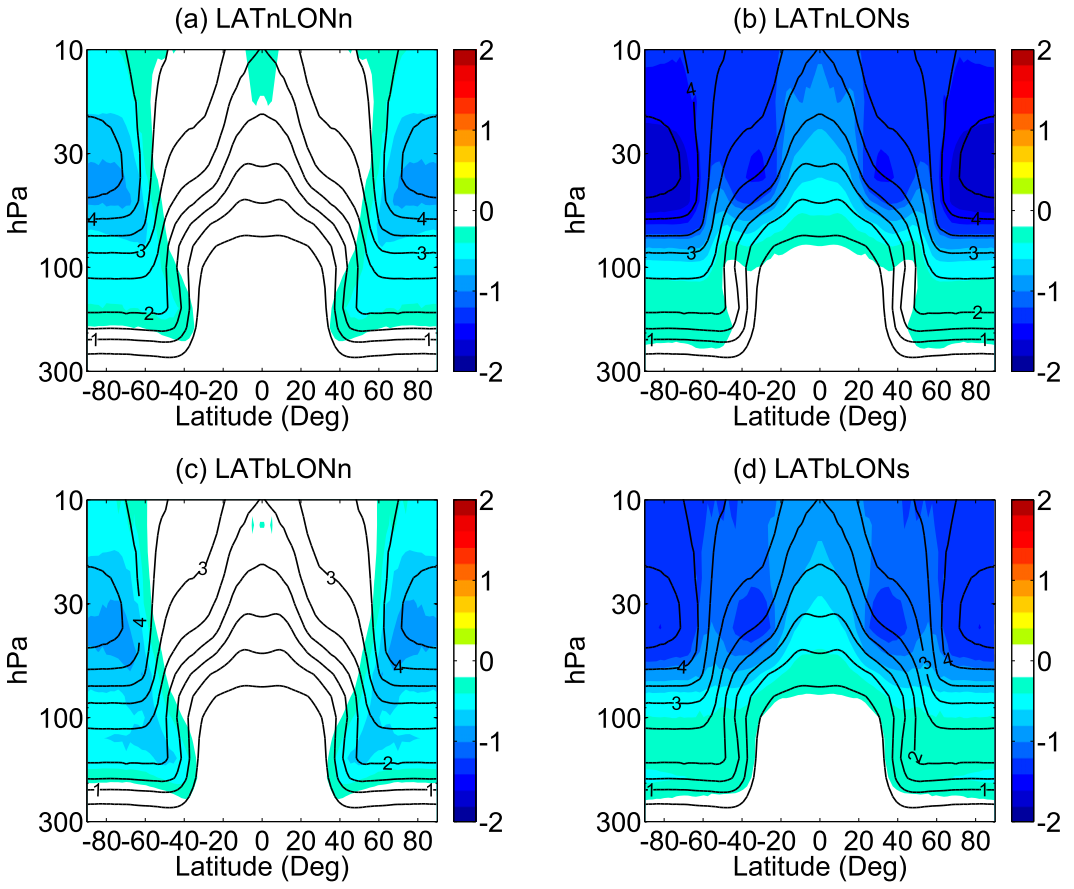

FIG. 5. As in Fig. 3, but for the mean AOA (yr). Note that the vertical axis has been changed to 10–300 hPa.

LATn heating but the jet shifts poleward when the meridional width of the heating is increased in LATb. This is consistent with what was found in Lu et al. (2008) and Chen et al. (2010), who argued that the differences between LATn and LATb are analogous to the jet response for El Niño forcing versus global warming.

Changes in zonal wind and temperature are accompanied by changes in stratospheric transport and mixing. The stratospheric mean diabatic circulation, denoted by the residual streamfunction, is strengthened above 100 hPa in all four experiments (Fig. 4). However, the spatial pattern of the strengthening depends critically on the zonal distribution of the SST forcing. LONn heating (left column) drives a shallow strengthening of the residual circulation, while LONs heating (right column) generates a deep acceleration of the BDC. Interestingly, the latitudinal extent of the heating has little effect on the stratospheric circulation response, although it alters the position of the tropospheric subtropical jet (cf. Fig. 3). The change in the residual circulation is also in agreement with the tropical temperature adjustment noted above, as expected from the thermodynamical balance in Eq. (7). In addition, an intensification of the tropical upwelling in the lower stratosphere is accompanied by an upward shift of the tropical tropopause, as well as a decrease in the cold point temperature, which in turn produces the upper-troposphere warming/lower-stratosphere cooling dipole pattern shown in Fig. 2. More importantly, while the climatological diabatic circulation exhibits a single hemispherical cell in the stratosphere, the different depths of the residual circulation response suggest distinct dynamical controls of the diabatic circulation. In a different idealized model, Gerber (2012) also found a tropospheric control of the shallow branch of the BDC by surface topographic forcing, and a stratospheric control of the deep branch by the intensity of the polar vortex. Our results suggest that a zonally symmetric SST forcing can also control the deep branch of the BDC through the strength of the subtropical jet and the associated thermal wind aloft, while a zonally localized SST forcing can control the shallow branch by convection-induced planetary waves.

It should be noted that Birner and Bönisch (2011) found that the deep branch of the stratospheric residual

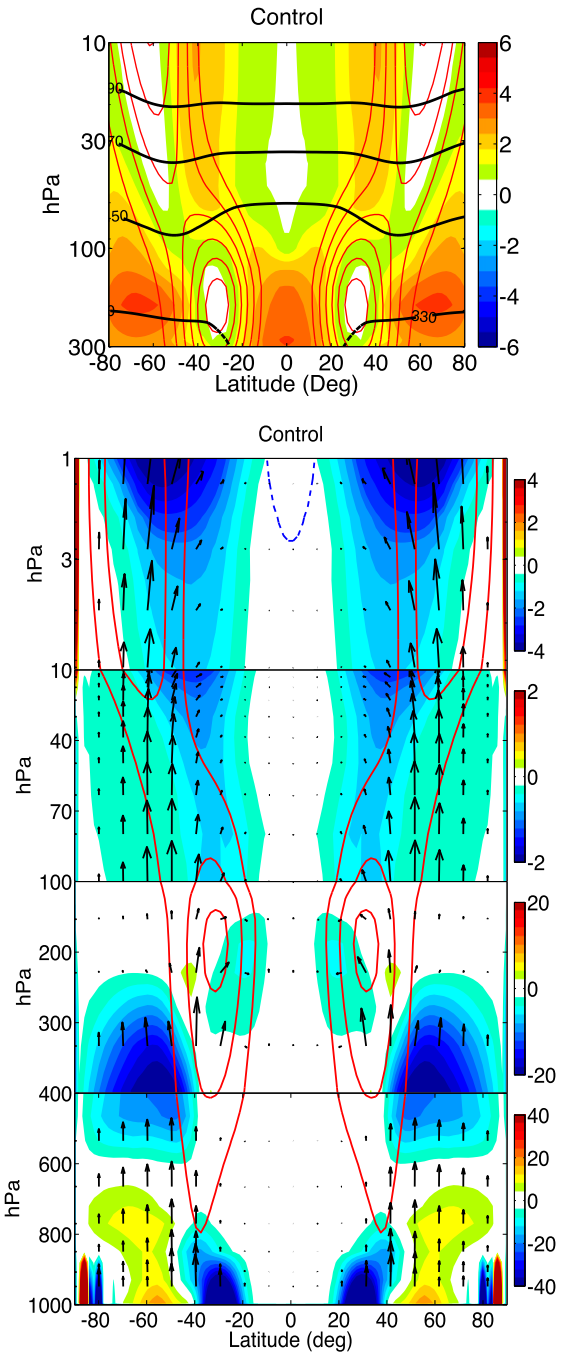

FIG. 6. (top) Climatology of the control run for the isentropic mixing denoted by the logarithm of equivalent length ratio $\tilde{\kappa}_{\text{eff}}$ (shading) and zonal mean zonal wind (m s^{-1}; colored contours). Several isentropic surfaces are highlighted as bold black lines to show where the equivalent length ratio data are originally interpolated from. (bottom) As above, but for EP flux (vectors) and associated divergence DF ($\text{m s}^{-1}\,\text{day}^{-1}$; shading), and zonal mean zonal wind (red contours: westerly wind, blue contours: easterly wind. Contour interval: $16\,\text{m s}^{-1}$). Warm shading denotes divergence (wave generation) and cold shading denotes convergence (wave dissipation). Note a change in the vertical axis.

circulation is generally broader in meridional width than the shallow branch, which seems to be opposite to our results. In fact, the meridional width of the shallow branch simulated in this study is consistent with the one in Birner and Bönisch (2011) within the latitudinal band equatorward of 70°N/S, and then the difference lies in the deep branch. One important factor that can cause this difference in the deep branch is the strength of the stratospheric polar vortex. As noted in section 2c, the polar vortex is much stronger due to the absence of stationary waves in the control run. Thus, the descending branch of the deep circulation takes place near the edge of the polar vortex, which in turn greatly limits the meridional width of the deep branch (see Fig. 2 in Plumb 2002). Also, it seems that the anomalous residual circulation cell near 60°N/S in LONn heating runs could be counted as a deep response if smaller values of contours are plotted in Figs. 4a and 4c. However, we argue that it should not be regarded as a deep response for the entire BDC, as it seems to be disconnected from the tropical upwelling that determines the hemispheric mass transport in the stratosphere along the deep branch of BDC.

The changes in the residual circulation have important consequences for the mean AOA in the stratosphere (cf. Fig. 5). Given an acceleration of the lower-stratospheric tropical upwelling in all four experiments, the mean AOA is reduced along the trajectory of the diabatic circulation. Therefore, in spite of the varied depths of the BDC change, the stratospheric air becomes fresher at the location of the polar vortex. Furthermore, with a deeper strengthening of the residual circulation for LONs heating, the mean AOA declines dominantly in the tropics and subtropics in addition to the extratropical decrease (cf. Figs. 5b,d). This low-latitude freshening of stratospheric air is small in the absolute change or relative change for LONn heating due to the absence of the tropical deep branch response in the BDC (cf. Figs. 4a,c). Again, the response of the mean AOA in the stratosphere does not depend on the latitudinal width of the SST heating, consistent with the change in the residual circulation.

Besides the mean diabatic circulation, the isentropic mixing can also be influenced by the tropical SST perturbation. The corresponding changes in isentropic mixing to different tropical SST forcings are shown in Fig. 7. Similar to the changes in the stratospheric residual circulation and AOA, the changes in isentropic mixing in the upper troposphere/lower stratosphere (UTLS) region are more strongly influenced by the zonal distribution of the tropical heating than by its latitudinal width. The anticorrelation between the changes in isentropic mixing and the zonal mean zonal flow still holds qualitatively. For LONn heating, isentropic mixing is predominantly

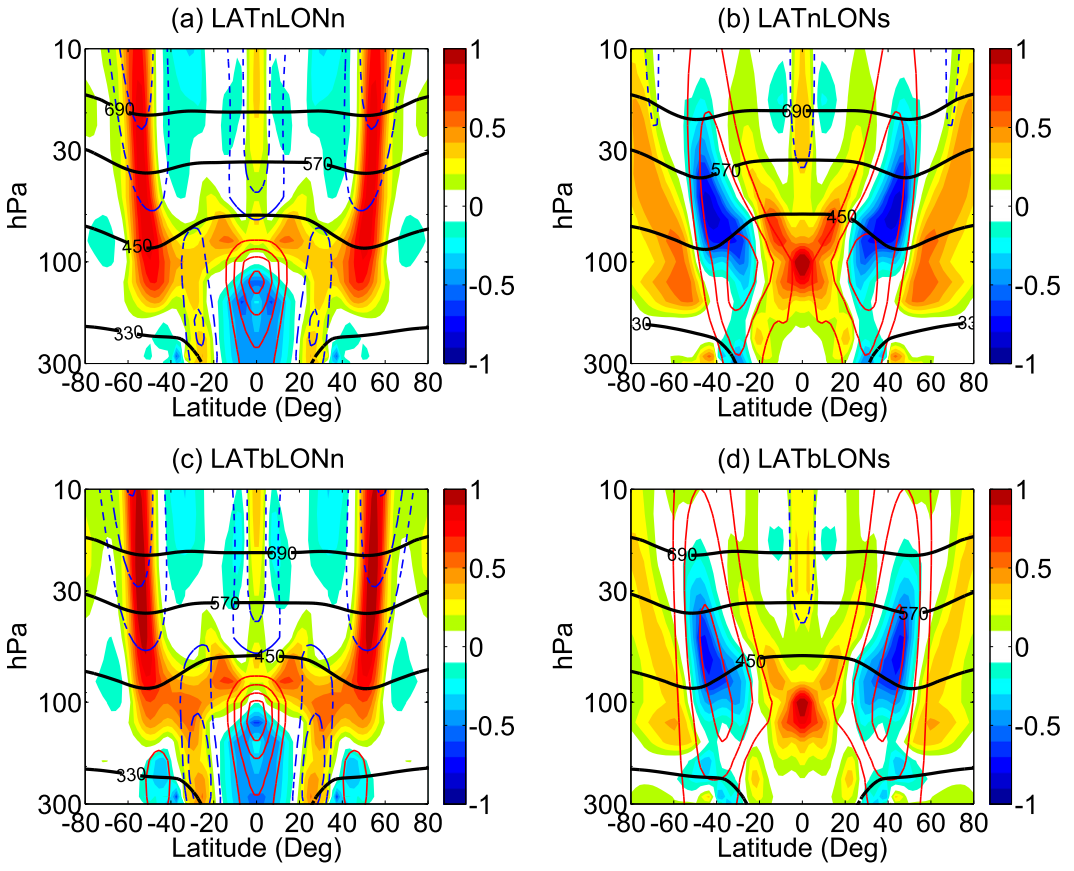

FIG. 7. As in Fig. 6 (top), but for the isentropic mixing anomalies. The contour interval is 4 m s^{-1}.

increased in the regions where westerlies are strongly suppressed including the stratospheric jet and the tropospheric subtropical jet. The decrease in isentropic mixing in the tropical upper troposphere can be attributed to the appearance of equatorial superrotation. On the contrary, for LONs heating, isentropic mixing decreases within the cores of upward-shifted and intensified subtropical jets. These changes in isentropic mixing can impact the mean AOA in the stratosphere. In addition to the Lagrangian trajectory and transit time determined from the residual circulation, isentropic mixing will increase the transit time by moving air parcels horizontally away from their trajectories. Overall, by a comparison of the mean AOA change with the change in the diabatic circulation and isentropic mixing, the change in stratospheric mean AOA seems to be dominated by the change in the residual circulation (as will be discussed in section 4b).

In summary, the BDC response to longitudinally narrow (LONn) heating differs from its counterpart with longitudinally symmetric (LONs) heating in many aspects. Particularly, LONn heating generates a shallow acceleration of the residual circulation, while LONs heating generates a deep strengthening of the BDC. This difference in the residual circulation change impacts the dynamical response in terms of stratospheric temperature and zonal wind, resulting in a much broader reduction of mean AOA in the lower stratosphere in the LONs experiments. The change in isentropic mixing also corresponds to the change in zonal wind. Moreover, by varying the latitudinal extent of the heating, the tropospheric subtropical jet transitions between an equatorward El Niño–like shift and a poleward global warming–like change, but the jet shift in latitude has little impact on the diagnostics of stratospheric transport. Therefore, we will focus on the effect of the zonal distribution of the SST forcing on the BDC in the remainder of this study.

4. Sensitivity of the BDC response to tropical SST forcing

a. *Sensitivity study*

Here we summarize briefly the robustness of the shallow-to-deep transition in the BDC response to the

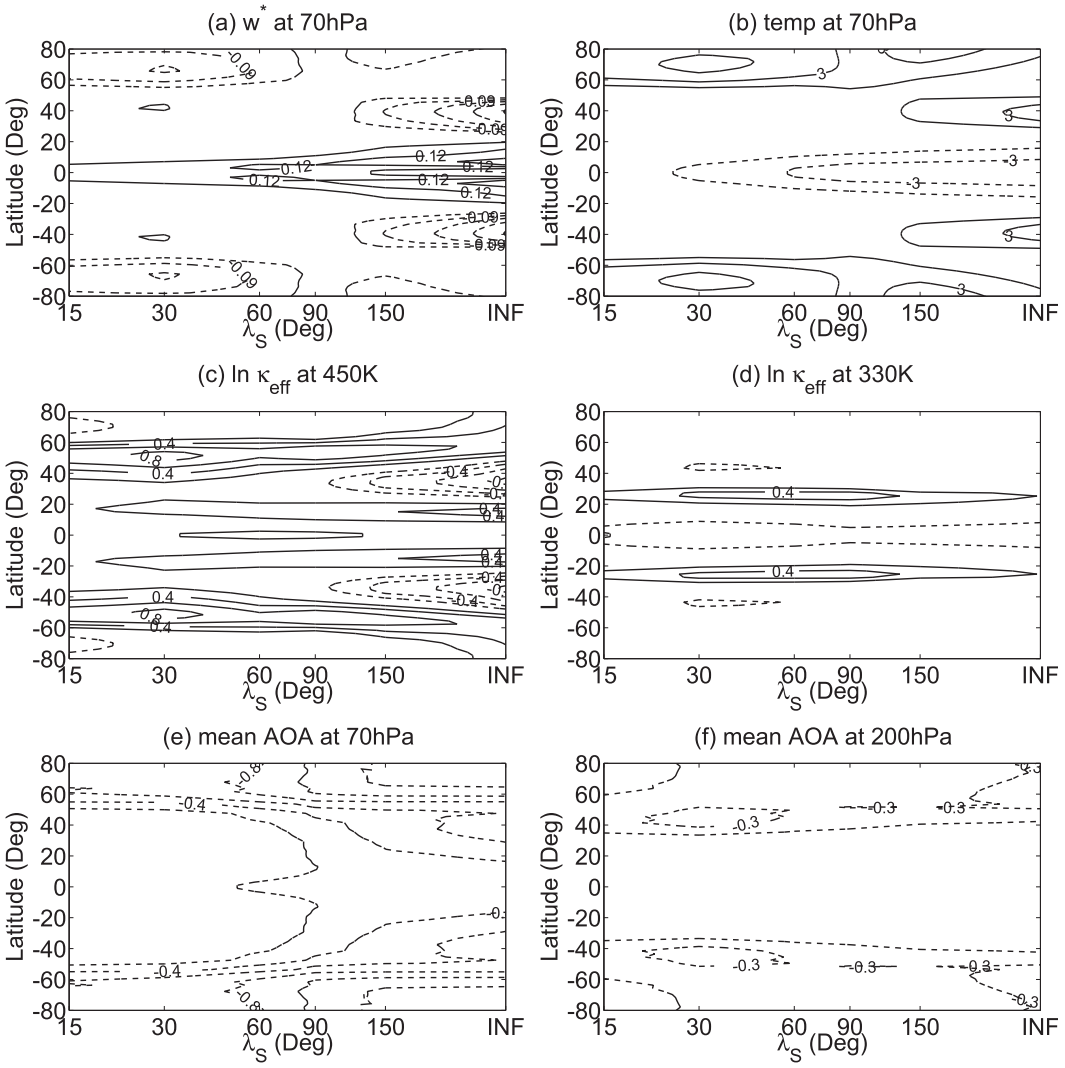

FIG. 8. Atmospheric changes following the expansion of the longitudinal extent λ_S for the LATn heating: (a) residual vertical velocity $\overline{w}^*$ at 70 hPa denoting the structural change in the BDC; (b) zonal mean temperature change at 70 hPa; (c),(d) isentropic mixing denoted by the logarithm of the equivalent length ratio $\tilde{\kappa}_{\text{eff}}$ on isentropic surfaces of 450 and 330 K, respectively, approximately equivalent to 70 and 200 hPa; and (e),(f) mean AOA at 70 and 200 hPa, respectively.

zonal distribution of the tropical SST forcing. Figure 8 displays the change in the stratospheric transport as a function of the zonal distribution of tropical SST heating (LONn corresponds to $\lambda_S = 30°$ and LONs corresponds to $\lambda_S = \infty$) for the latitudinally narrow (LATn) heating experiments. The eddy mixing anomaly is denoted by the equivalent length ratio $\tilde{\kappa}_{\text{eff}}$ on isentropic surfaces, and the rough correspondence between isentropic surfaces and pressure surfaces can be seen in Fig. 6. For all the experiments with $\lambda_S < 90°$, the residual vertical velocity $\overline{w}^*$ at 70 hPa exhibits anomalous upwelling in deep tropics and downwelling over the polar regions. Particularly, the anomalous downwelling occurs within the polar vortex, highlighting an extratropical response. As expected from a thermodynamical balance, temperature anomalies mirror the changes in residual vertical velocity, with cooling corresponding to strengthened upwelling at the equator and warming corresponding to strengthened downwelling at the poles. Moreover, positive anomalies of the equivalent length ratio $\tilde{\kappa}_{\text{eff}}$ are found at the 450-K isentropic surface over the midlatitude region. This indicates increased isentropic mixing in the midlatitude lower stratosphere, consistent with a weakened polar vortex and polar warming. Subject to these changes, the mean AOA is reduced over the polar vortex. All of these characteristics are

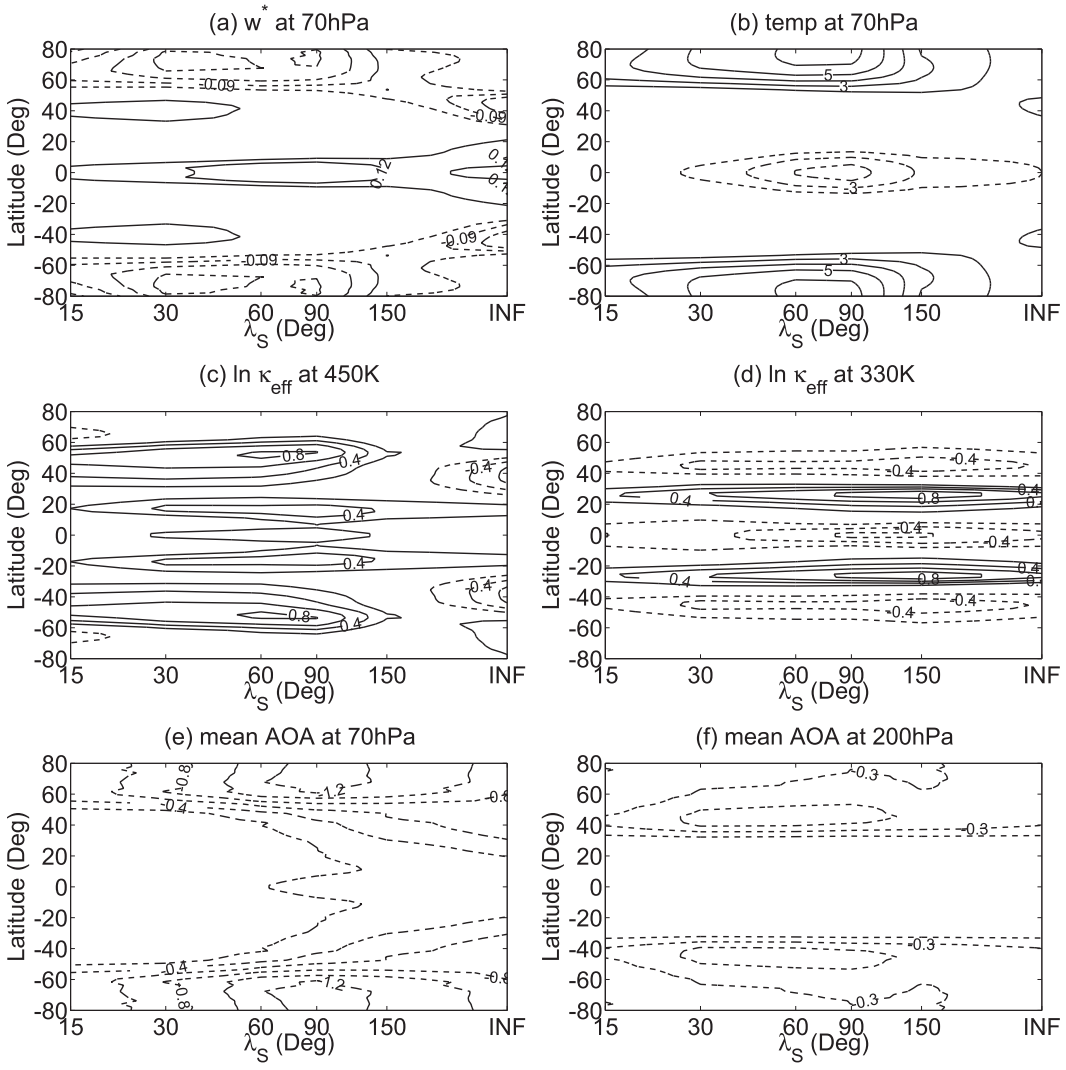

FIG. 9. As in Fig. 8, but for the LATb heating.

consistent with the LONn experiments described in section 3.

For all the experiments with $\lambda_S > 90°$, although $\overline{w}^*$ at 70 hPa also exhibits an anomalous upwelling in the deep tropics, the center of anomalous downwelling moves from the high latitudes to the midlatitudes (Fig. 8a), stressing a tropical and subtropical strengthening of the residual circulation as seen in Figs. 4b and 4d. Temperature anomalies also show dynamical warming in the midlatitudes mirroring the increased downwelling. Interestingly, the isentropic mixing at the 450-K isentrope is strongly suppressed in the surf zone, which can be attributed to the upward shift and intensification of the subtropical jets. Accompanying these circulation changes is a broad decline of the mean AOA in the lower stratosphere extending into the deep tropics. All of these features are consistent with the LONs experiments.

It is noteworthy that the transition in the lower-stratospheric transport takes place abruptly around the value of $\lambda_S = 90°$. Such a clear transition is not observed in the upper troposphere. A number of additional experiments are performed to confirm the robustness of the shallow-to-deep transition by exploring the parameters in the SST perturbation. The same diagnostics are presented in Fig. 9 for the latitudinally broad (LATb) heating. A likewise transition is observed in the lower-stratospheric residual circulation, temperature, isentropic mixing, and mean AOA with the zonal asymmetry of tropical heating, which are consistent with the changes in the stratospheric polar vortex (not shown). Although the transition is qualitatively similar, the threshold value

of the zonal extent ($\lambda_S = 150°$) is larger than that for LATn forcing. Other than that, the increase in tropical upwelling is not monotonic with the longitudinal extent λ_S, but a maximum is observed in the cooling of the deep tropics for $\lambda_S = 60°$–$90°$.

Furthermore, as the zonally averaged SST heating is much smaller in the LONn runs as compared to the LONs runs, we have conducted sensitivity experiments by increasing the SST heating amplitude in the LONn heating A_0 to match the zonal mean SST heating magnitude of the LONs run. Despite a much stronger local SST forcing, the new LONn run yields a qualitatively similar shallow circulation response in residual circulation and associated changes in zonal wind, as well as isentropic mixing (not shown). Finally, we have shifted the latitude of the maximum SST heating, ϕ_0, away from the equator as in Norton (2006). The BDC response is qualitatively similar, while the magnitude of the response is gradually reduced as the heating center moves away from the equator (not shown). Overall, our sensitivity study confirms the robustness of the transition from a shallow branch response to a deep response with respect to the distribution of the tropical SST forcing, although the threshold of the transition can be sensitive to the structure or magnitude of the SST forcing.

b. *Linkage between the residual circulation, isentropic mixing, and AOA*

Using these sensitivity experiments, we will test the dynamical linkage between the mean residual circulation, isentropic mixing, and the AOA by a simple correlation analysis. In section 3, we found that the stratospheric mean AOA change can be explained qualitatively by the change in the residual circulation. Given the experiments with separate changes in the zonal asymmetry and meridional width of tropical SST heating, we will test the dynamical relationship quantitatively. In particular, to what extent can a change in AOA be explained by the mean circulation versus the eddy mixing? Empirically, we found that the strength of tropical upwelling is well correlated with AOA in most of the stratosphere, and that the eddy mixing has almost no local correlation with AOA except near the subtropical tropopause. Here we present the results for remote and local effects on the mean AOA in two regions: the polar vortex region (averaged between 60° and 65°N at 70 hPa) and near the subtropical tropopause (averaged between 40° and 45°N at 200 hPa).

Figure 10 compares the mean AOA changes in the two regions with the changes in tropical upwelling (i.e., $\overline{w}^*$ averaged between 15°S and 15°N at 70 hPa) and local eddy mixing (i.e., the equivalent length of PV). For the AOA near the polar vortex (top row), the AOA is well correlated with the strength of tropical upwelling ($R^2 = 0.64$), but it displays almost no correlation with the strength of local eddy mixing. The experiment with larger tropical upwelling also corresponds to fresher air near the polar vortex, as expected from the transport by the overturning circulation from the tropics to the poles. This relationship holds for both LATn and LATb. This suggests statistically that when the tropical SSTs are perturbed, the strength of tropical upwelling has a dominant control on the polar AOA in the lower stratosphere over the effect of local mixing.

As for the mean AOA near the subtropical tropopause, the AOA exhibits almost no correlation with the strength of tropical upwelling in this case (Fig. 10c), but it is well correlated with the strength of eddy mixing on the equatorward flank of the subtropical jet, yielding $R^2 = 0.52$ (Fig. 10d). The experiment with larger isentropic mixing near the subtropical tropopause corresponds to fresher air locally. This can be explained by a rapid exchange of air masses near the tropopause associated with Rossby wave breaking, and the resulting freshening of air is more efficient in ventilating the air near the tropopause than the mean overturning circulation in the lower stratosphere.

5. Mechanisms of the residual circulation and isentropic mixing changes

In this section, we further investigate the mechanisms of the stratospheric transport changes in response to the distribution of tropical heating. Figure 11 compares the residual vertical velocities at 70 hPa from the TEM definition $\overline{w}^*$ (solid), the momentum balance via the "downward control" mechanism $\overline{w}^*_m$ (dashed), and the thermodynamic balance $\overline{w}^*_Q$ (dash-dotted). The anomalies are compared with the climatological residual vertical velocity in the control run scaled by a factor of 1/3 (thin solid line). For all SST forcings, the anomalies of $\overline{w}^*$, $\overline{w}^*_m$, and $\overline{w}^*_Q$ show a qualitatively good agreement with each other. This confirms that the acceleration of the residual circulation in the lower stratosphere in our SST experiments is eddy-driven and that the eddy-driven circulation is consistent with the diabatic heating change. Moreover, compared with the climatological single cell with tropical upwelling and extratropical downwelling, LONn heating tends to establish two anomalous cells (Figs. 11a,c). One anomalous cell lies in the climatological upwelling zone and the other is located in the downwelling zone, which is consistent with the residual streamfunction changes shown in Figs. 4a and 4c. In particular, the anomalous downwelling in the high latitudes is associated with an anomalous upwelling in the midlatitudes. By contrast, for LONs heating (Figs. 11b,d),

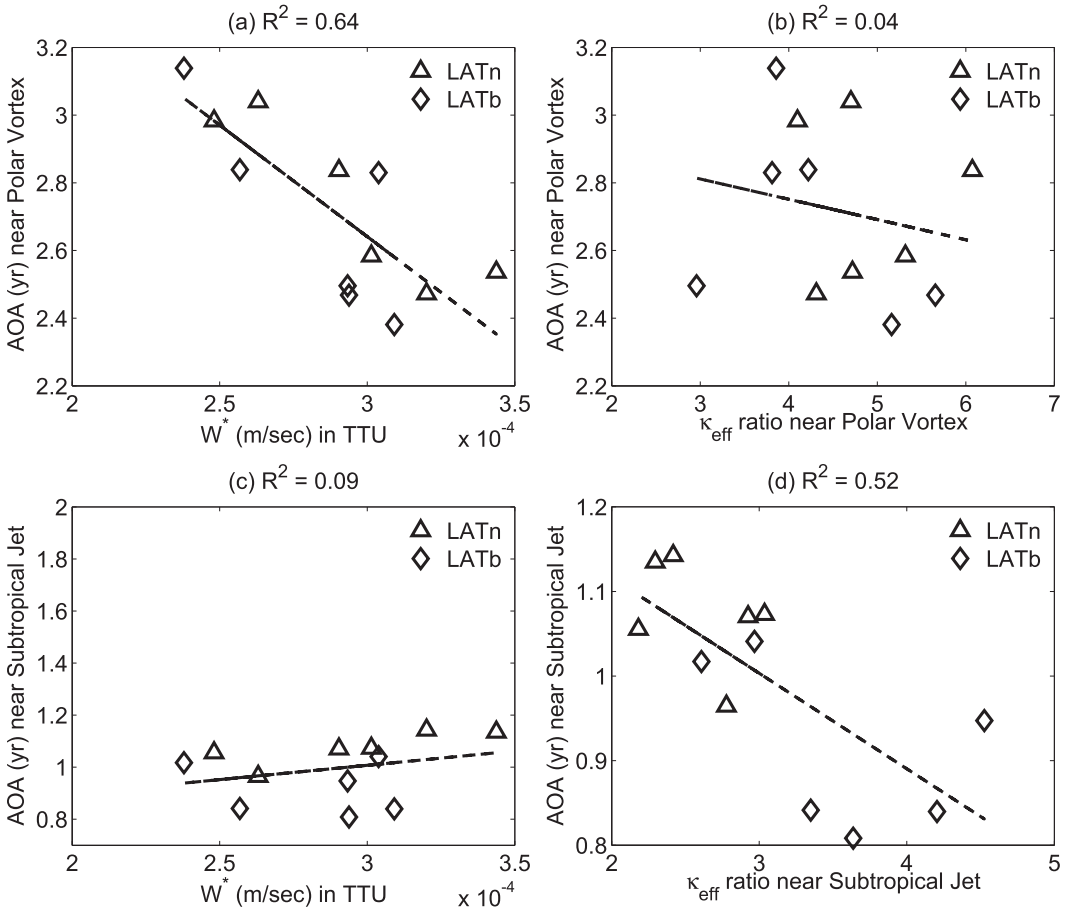

FIG. 10. Scatterplots examining the correlation between (a) the strength of the BDC and mean AOA at the polar vortex; (b) the strength of isentropic eddy mixing at the edge of the polar vortex and mean AOA at the polar vortex; (c) the strength of the BDC and mean AOA on the poleward side near the subtropical jet; and (d) the strength of isentropic eddy mixing and mean AOA both near the subtropical jet. Here, the strength of the BDC is denoted by the residual vertical velocity $\overline{w}^*$ ($\mathrm{m\,s^{-1}}$) in the tropical tropopause upwelling (15°S–15°N, 70 hPa); the strength of isentropic eddy mixing is assessed by the equivalent length ratio $\tilde{\kappa}_{\mathrm{eff}}$ at the northern subtropical jet (25°–30°N, 330 K) and the edge of the northern polar vortex (55°–60°N, 450 K) separately; and, last, the mean AOA (yr) is averaged near the subtropical jet (40°–45°N, 200 hPa) and at the polar vortex (60°–65°N, 70 hPa). Experiments with LATn and LATb heating are marked as Δ and ◇, respectively.

the residual vertical velocities anomalies intensify the climatological mean pattern of tropical upwelling and extratropical downwelling, consistent with Figs. 4b and 4d. In summary, the shallow residual circulation response to the LONn heating is accompanied by an anomalous tropical cell and an extratropical cell out of phase with the climatological mean pattern, and the deep response to the LONs heating is associated with an anomalous equator-to-pole cell reinforcing the mean pattern.

Which mechanisms drive the distinct residual circulation changes with respect to the distribution of SST forcing? In the climatological mean (Fig. 6, bottom), planetary waves propagate into the stratosphere and are dissipated in the midlatitude surf zone, driving the residual circulation through the downward control mechanism. For LONn heating (Figs. 12a,c), the deep convection generates stationary planetary waves in tropical upper troposphere. Additionally, the prescribed SST perturbation alters the extratropical baroclinity. This acts to generate more transient waves at the lower boundary, including both synoptic waves and planetary waves. The convection-induced stationary planetary waves not only dissipate heavily in the tropical lower stratosphere, but also propagate away from their source and dissipate in the extratropical stratosphere. The extratropical transient waves, on the other hand, experience less dissipation in the midlatitude troposphere (40°–60°N/S, 200–400 hPa), resulting in increased dissipation in the stratosphere. The tropical cell of anomalous residual circulation (cf. Figs. 4a,c) is primarily due to the

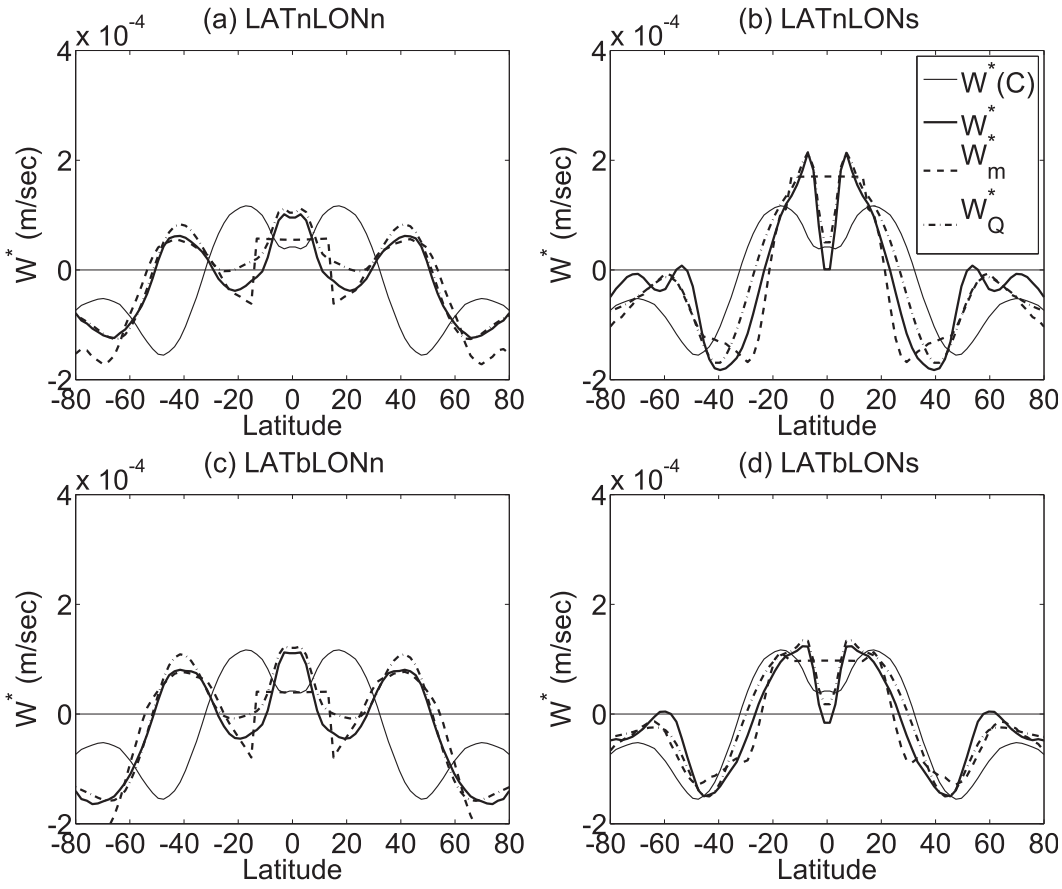

FIG. 11. Anomaly of the residual vertical velocity at 70 hPa ($m\,s^{-1}$) from different definitions, $\overline{w}^*$ (thick line); from downward control (i.e., dynamic balance), $\overline{w}^*_m$ (dashed line); and from thermodynamic balance, $\overline{w}^*_Q$ (dash–dotted line). The corresponding climatological $\overline{w}^*$ [W*(C) in the legend] in the control run is shown as the thin solid line and has been scaled by a factor of 1/3. The anomalies are plotted for (a) LATnLONn, (b) LATnLONs, (c) LATbLONn, and (d) LATbLONs.

convection-induced stationary waves while the extratropical cell is attributed to changes in both convection-induced stationary waves and extratropical transient waves (not shown here).

For LONs heating (Figs. 12b,d), there is also an anomalous EP flux divergence in the upper troposphere. The change in EP flux roughly follows the shift of the subtropical jet, and therefore the maximum anomalous divergence occurs on the equatorward side of 40°N for LATn heating and on the poleward side of 40°N for LATb heating at 200–400 hPa. In contrast to the responses to LONn heating, the upward propagation of these waves is not directly accompanied by an EP flux convergence between 40 and 100 hPa, where the zonal wind is increased considerably due to the upward shift of the subtropical jet. Instead, the planetary waves propagate either more equatorward or upward from these regions of enhanced zonal winds, which in turn drives a deeper overturning circulation (Figs. 4b,d).

Given the remarkable similarity between the stratospheric circulation in the LATn and LATb runs, the generation and propagation of waves in the troposphere are of secondary importance in comparison with the eddy propagation and dissipation in the stratosphere, which drives distinct responses in the residual circulation between LONn and LONs heating. The lower stratospheric response is therefore investigated further: a key difference between the shallow and deep responses in the residual circulation appears in the EP flux convergence (i.e., the eddy dissipation) in the subtropical lower stratosphere. With all the sensitivity experiments examined in section 4, we further found a strong correlation in the lower stratosphere between the meridional component of the EP flux in the midlatitudes (40°–60°) and the strength of subtropical eddy dissipation, suggesting that an increased equatorward propagation of midlatitude waves in the lower stratosphere leads to more eddy dissipation in the subtropics.

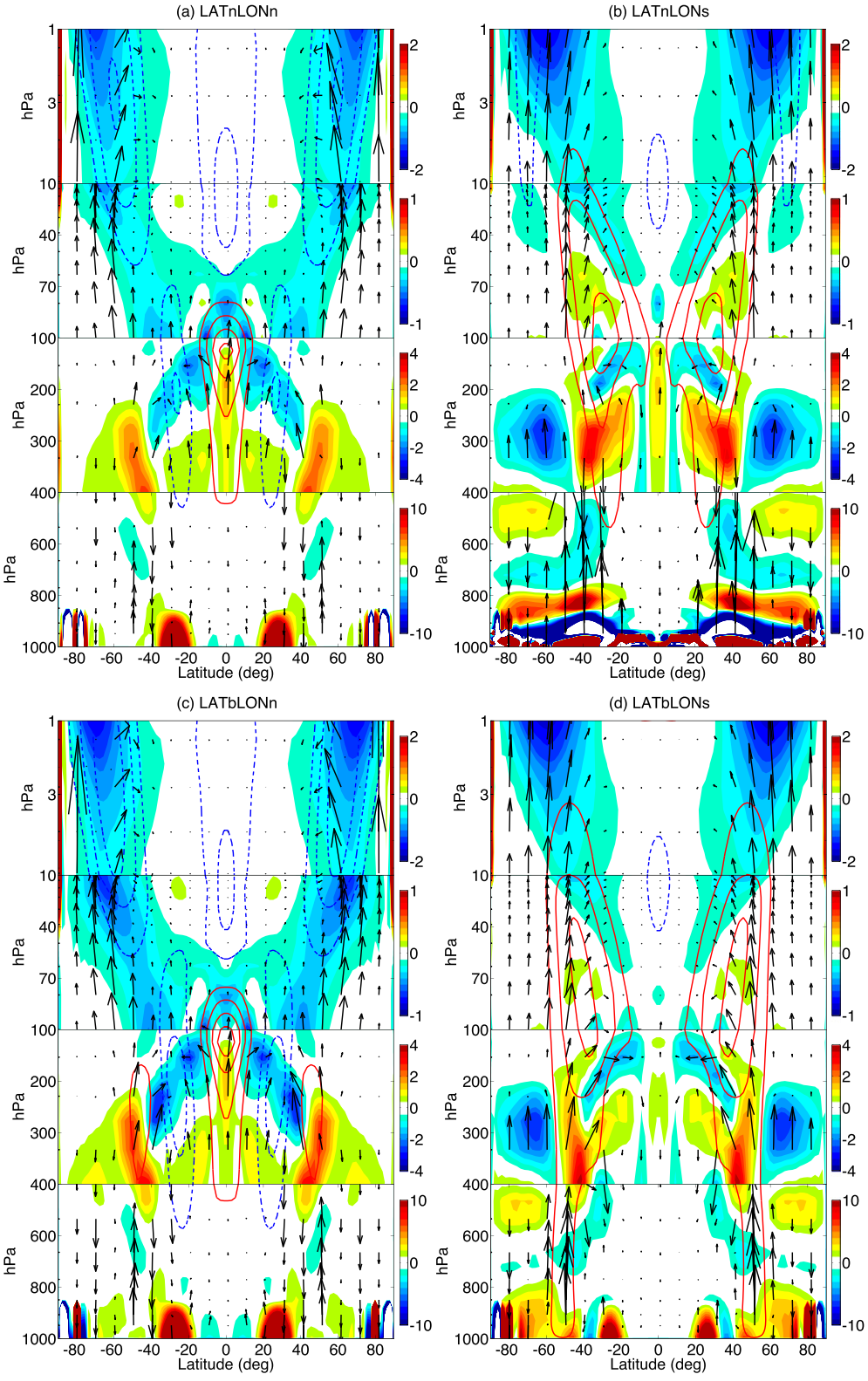

FIG. 12. As in Fig. 3, but for the EP flux (vectors) and associated divergence DF ($m\,s^{-1}\,day^{-1}$; shading), and zonal mean zonal wind ($m\,s^{-1}$; contours). The contour interval is $4\,m\,s^{-1}$. Note that the vertical axis has been changed to 1–1000 hPa.

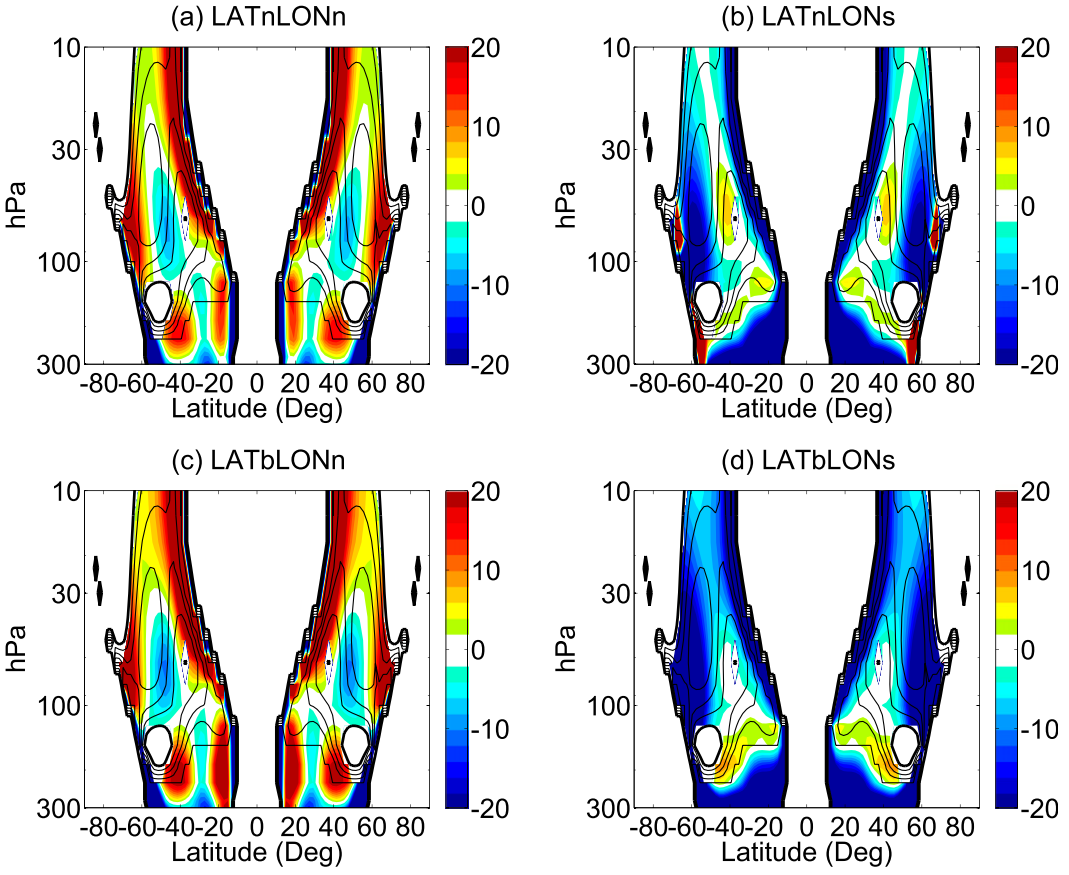

FIG. 13. Anomaly of the refractive index for (a) LATnLONn, (b) LATnLONs, (c) LATbLONn, and (d) LATbLONs, with the corresponding climatology in the control run shown as contours (interval: 10). The bold contour indicates both the zero line and the critical line, separating the regions of propagation from those of no propagation. In the lower stratosphere, the climatological minimum is near 40°N/S, whereas the climatological maximum is more poleward and near 50°N/S.

The changes in eddy propagation can be explained by a change in the refractive index of Rossby waves n^2 (Fig. 13). Eddies are able to propagate in regions of positive refractive index n^2, and they propagate from the regions of low values of the refractive index to the regions of high index values. Our calculation of the refractive index follows Matsuno (1970). For the transient planetary waves that are dominant in our model, we set the value of the eddy phase speed to $c_p = 5\,\mathrm{m\,s^{-1}}$, and the zonal wavenumber to $k = 3$. The results are qualitatively similar for choosing the wavenumber $k = 2$ or 4, or for a moderate variation of the phase speed c_p, and the conclusions made here are also valid for the stationary planetary waves, which are important for LONn heating response.

For the LONn heating (Figs. 13a,c), pronounced negative anomalies of the refractive index n^2 are found at 40°–50° whereas positive anomalies are found poleward of 60° near and above 100 hPa. This enhances the meridional gradient of the refractive index from a minimum in the midlatitudes to a maximum at the edge of the polar vortex (contours in Figs. 13a,c). Considering that the majority of the anomalous waves penetrating the tropopause reside poleward of 50° (cf. Figs. 12a,c), the enhanced meridional gradient of the refractive index prevents equatorward wave propagation and guides these waves poleward. As the waves are approaching the critical line near the edge of the polar vortex, the waves break down and dissipate, driving a shallow, extratropical strengthening of the residual circulation. On the contrary, for the LONs heating (Figs. 13b,d), the anomaly in the refractive index results in a decline or even reversal of the climatological meridional gradient of the refractive index (not shown). Given that the majority of anomalous waves penetrating the tropopause resides equatorward of 50° for LONs heating (cf. Figs. 12b,d), the declined or reversed meridional gradient of the refractive index forces these anomalous waves to propagate equatorward and to dissipate near the critical line in the subtropical lower stratosphere. Consequently,

this leads to a deeper and broader strengthening of the residual circulation. We have further decomposed the refractive index n^2 into the meridional wavenumber l and vertical wavenumber m using the diagnostic described in Harnik and Lindzen (2001) (figures not shown here). The results confirm an equatorward shifted zone of meridional wave propagation given by l^2 and further an equatorward EP flux convergence in the middle and upper stratosphere (1–10 hPa) given by m^2 for LONs heating. This diagnostic suggests that the distinct responses of stratospheric eddy dissipation between LONn and LONs heating are indeed due to different pathways of eddy propagation in the stratosphere, which cause different types of strengthening of the stratospheric residual circulation.

With a simple diffusive closure, one can relate the pattern of EP flux divergence to the isentropic mixing of PV (Yang et al. 1990). Thus, it can be expected that the simulated changes in isentropic mixing are associated with changes in eddy dissipation through Rossby wave breaking. This can be confirmed by the increase in isentropic mixing near the stratospheric jets (50°–60°) (shading in Figs. 7a,c), which overlaps with the region of extratropical anomalous EP flux convergence (shading in Figs. 12a,c) for LONn heating. Similarly, the regions of decreased isentropic mixing within the surf zone (20°–40°) (shading in Figs. 7b,d) overlap with the region of subtropical anomalous EP flux divergence (shading in Figs. 12b,d) for LONs heating.

As noted in section 3, we also find that the response of the isentropic mixing to tropical SST forcing generally mirrors the changes in zonal mean zonal wind in all our experiments (cf. Fig. 7). Although both EP flux convergence and the zonal wind vary consistently with the changes of isentropic mixing in the stratosphere, it is interesting to note that changes in the zonal wind seem to be a better predictor of the changes in eddy mixing than the EP flux convergence in the troposphere. For example, there is a significant decrease in isentropic mixing in the tropical upper troposphere (cf. Figs. 7a,c) for LONn heating that mirrors the eastward acceleration of equatorial zonal mean zonal winds. This effect dominates over the increased local eddy dissipation (cf. Figs. 12a,c) in favor of a larger mixing. This seems to be consistent with simple kinematic models of tracer transport with a prescribed jet and stochastic noise, which suggests that the jet structure has a dominant control on tracer mixing (Haynes et al. 2007).

6. Summary and discussion

The sensitivities of the BDC to tropical SST heating are investigated in an idealized aquaplanet model. It is found that an increase in tropical SSTs generally leads to an acceleration of tropical upwelling and an associated reduction in AOA in the polar stratosphere. AOA near the subtropical tropopause is correlated with local isentropic mixing of tropospheric and stratospheric air. The spatial distribution of the SST forcing influences stratospheric transport including the diabatic circulation, AOA, and isentropic mixing. More specifically, while the locations of tropospheric wave generation and propagation depend on the meridional width of the SST heating (see also Chen et al. 2010), the zonal distribution of SST perturbations has a more pronounced impact on the vertical and meridional structures of transport and mixing in the stratosphere: Longitudinally narrow (LONn) SST heating tends to generate a shallow acceleration of the stratospheric residual circulation, enhanced isentropic mixing associated with a weakened stratospheric jet, and a reduction in the AOA mostly within the polar vortex. By contrast, longitudinally symmetric (LONs) SST heating tends to produce a deep strengthening of the stratospheric residual circulation, suppressed isentropic mixing associated with a stronger stratospheric jet, and a decline of AOA in the entire stratosphere. As the SST perturbation is gradually varied from zonally localized to zonally symmetric, the shallow residual circulation response abruptly transitions to a deep response. Gerber (2012) also found a tropospheric control of the shallow branch of the BDC by surface topographic forcing, and a stratospheric control of the deep branch by the intensity of the polar vortex. Our results suggest that a zonally symmetric SST heating can also control the deep branch of the BDC through the strength of the subtropical jet and the associated thermal wind aloft, while tropical SST heating localized in longitude can control the shallow branch by convection-induced planetary waves. Therefore, while our idealized model simulation corresponds to the annual mean circulation for simplicity, a similar mechanism can operate in the winter stratosphere where the stratosphere–troposphere coupling is more active with stationary waves.

The changes in the residual circulation are induced by the planetary wave drag through the downward control mechanism (Haynes et al. 1991). Although the meridional width of tropical SST heating influences the locations of baroclinic wave generation and propagation, it is the wave propagation and dissipation in the subtropical lower stratosphere that are responsible for the depth of the stratospheric residual circulation response. Zonally localized SST heating weakens the stratospheric jet and guides the planetary waves poleward in the lower stratosphere, leading to a shallow change in the residual circulation. By contrast, the zonal wind response to zonally symmetric SST heating is characterized by an

upward shift of the subtropical jet, which in turn refracts the planetary waves equatorward and upward in the lower stratosphere, leading to a deep change in the residual circulation. This also yields weaker isentropic mixing associated with a more robust transport barrier due to a stronger subtropical jet. Our results suggest that while the recent decadal changes in the shallow branch of the BDC (Bönisch et al. 2011) may be partially attributed to a more basinwide SST trend, the upward shift of the subtropical jet associated with zonally symmetric SST heating, as found in chemical climate model simulations under climate warming (Garcia and Randel 2008; McLandress and Shepherd 2009; Garny et al. 2011), can impact the deep branch of the BDC.

Acknowledgments. We thank Rolando Garcia, Peter Hess, Lantao Sun, and two anonymous reviewers for valuable discussions. Also, the authors thank Nili Harnik and Tiffany Shaw for providing their linear QG model to confirm the wave propagation characteristics. HY and GC are supported by the National Science Foundation (NSF) climate and large-scale dynamical program under Grant ATMS-0456157. DD is supported by the German Cluster of Excellence for Integrated Climate System Analysis and Prediction (CliSAP).

REFERENCES

Allen, D., and N. Nakamura, 2001: A seasonal climatology of effective diffusivity in the stratosphere. *J. Geophys. Res.,* **106** (D8), 7917–7935, doi:10.1029/2000JD900717.

Andrews, D., J. Holton, and C. Leovy, 1987: *Middle Atmosphere Dynamics*. Academic Press, 489 pp.

Birner, T., and H. Bönisch, 2011: Residual circulation trajectories and transit times into the extratropical lowermost stratosphere. *Atmos. Chem. Phys.,* **11,** 817–827, doi:10.5194/acp-11-817-2011.

Bönisch, H., A. Engel, T. Birner, P. Hoor, D. W. Tarasick, and E. A. Ray, 2011: On the structural changes in the Brewer–Dobson circulation after 2000. *Atmos. Chem. Phys.,* **11,** 3937–3948, doi:10.5194/acp-11-3937-2011.

Brewer, A. W., 1949: Evidence for a world circulation provided by the measurements of helium and water vapor distribution in the stratosphere. *Quart. J. Roy. Meteor. Soc.,* **75,** 351–363, doi:10.1002/qj.49707532603.

Butchart, N., and Coauthors, 2010: Chemistry–climate model simulations of twenty-first century stratospheric climate and circulation changes. *J. Climate,* **23,** 5349–5374, doi:10.1175/2010JCLI3404.1.

Calvo, N., R. R. Garcia, W. J. Randel, and D. R. Marsh, 2010: Dynamical mechanism for the increase in tropical upwelling in the lowermost tropical stratosphere during warm ENSO events. *J. Atmos. Sci.,* **67,** 2331–2340, doi:10.1175/2010JAS3433.1.

Chen, G., J. Lu, and D. M. W. Frierson, 2008: Phase speed spectra and the latitude of surface westerlies: Interannual variability and global warming trend. *J. Climate,* **21,** 5942–5959, doi:10.1175/2008JCLI2306.1.

——, R. A. Plumb, and J. Lu, 2010: Sensitivities of zonal mean atmospheric circulation to SST warming in an aqua-planet model. *Geophys. Res. Lett.,* **37,** L12701, doi:10.1029/2010GL043473.

Deckert, R., and M. Dameris, 2008: Higher tropical SSTs strengthen the tropical upwelling via deep convection. *Geophys. Res. Lett.,* **35,** L10813, doi:10.1029/2008GL033719.

Delworth, T. L., and Coauthors, 2006: GFDL's CM2 global coupled climate models. Part I: Formulation and simulation characteristics. *J. Climate,* **19,** 643–674, doi:10.1175/JCLI3629.1.

Dobson, G. M. B., 1956: Origin and distribution of the polyatomic molecules in the atmosphere. *Proc. Roy. Soc. London,* **236A,** 187–193, doi:10.1098/rspa.1956.0127.

Donner, L. J., and Coauthors, 2011: The dynamical core, physical parameterizations, and basic simulation characteristics of the atmospheric component AM3 of the GFDL global coupled model CM3. *J. Climate,* **24,** 3484–3519, doi:10.1175/2011JCLI3955.1.

Edmon, H. J., Jr., B. J. Hoskins, and M. E. McIntyre, 1980: Eliassen–Palm cross sections for the troposphere. *J. Atmos. Sci.,* **37,** 2600–2616, doi:10.1175/1520-0469(1980)037<2600:EPCSFT>2.0.CO;2.

Eichelberger, S. J., and D. L. Hartmann, 2005: Changes in the strength of the Brewer–Dobson circulation in a simple AGCM. *Geophys. Res. Lett.,* **32,** L15807, doi:10.1029/2005GL022924.

Engel, A., and Coauthors, 2008: Age of stratospheric air unchanged within uncertainties over the past 30 years. *Nat. Geosci.,* **2,** 28–31, doi:10.1038/ngeo388.

Garcia, R. R., and W. J. Randel, 2008: Acceleration of the Brewer–Dobson circulation due to increases in greenhouse gases. *J. Atmos. Sci.,* **65,** 2731–2739, doi:10.1175/2008JAS2712.1.

——, ——, and D. E. Kinnison, 2011: On the determination of age of air trends from atmospheric trace species. *J. Atmos. Sci.,* **68,** 139–154, doi:10.1175/2010JAS3527.1.

García-Herrera, R., N. Calvo, R. R. Garcia, and M. A. Giorgetta, 2006: Propagation of ENSO temperature signals into the middle atmosphere: A comparison of two general circulation models and ERA-40 reanalysis data. *J. Geophys. Res.,* **111,** D06101, doi:10.1029/2005JD006061.

Garny, H., M. Dameris, W. J. Randel, G. E. Bodeker, and R. Deckert, 2011: Dynamically forced increase of tropical upwelling in the lower stratosphere. *J. Atmos. Sci.,* **68,** 1214–1233, doi:10.1175/2011JAS3701.1.

Gerber, E. P., 2012: Stratospheric versus tropospheric control of the strength and structure of the Brewer–Dobson circulation. *J. Atmos. Sci.,* **69,** 2857–2877, doi:10.1175/JAS-D-11-0341.1.

Hall, T. M., and R. A. Plumb, 1994: Age as a diagnostic of stratospheric transport. *J. Geophys. Res.,* **99** (D1), 1059–1070, doi:10.1029/93JD03192.

Hardiman, S. C., N. Butchart, P. H. Haynes, and S. H. E. Hare, 2007: A note on forced versus internal variability of the stratosphere. *Geophys. Res. Lett.,* **34,** L12803, doi:10.1029/2007GL029726.

Harnik, N., and R. S. Lindzen, 2001: The effect of reflecting surfaces on the vertical structure and variability of stratospheric planetary waves. *J. Atmos. Sci.,* **58,** 2872–2894, doi:10.1175/1520-0469(2001)058<2872:TEORSO>2.0.CO;2.

Haynes, P., and E. Shuckburgh, 2000a: Effective diffusivity as a diagnostic of atmospheric transport: 1. Stratosphere. *J. Geophys. Res.,* **105** (D18), 22 777–22 794, doi:10.1029/2000JD900093.

——, and ——, 2000b: Effective diffusivity as a diagnostic of atmospheric transport: 2. Troposphere and lower stratosphere. *J. Geophys. Res.,* **105** (D18), 22 795–22 810, doi:10.1029/2000JD900092.

——, C. J. Marks, M. E. Mcintyre, T. G. Shepherd, and K. P. Shine, 1991: On the ''downward control'' of extratropical diabatic circulation by eddy-induced mean zonal forces. *J. Atmos. Sci.,* **48,** 651–678, doi:10.1175/1520-0469(1991)048<0651:OTCOED>2.0.CO;2.

——, D. A. Poet, and E. F. Shuckburgh, 2007: Transport and mixing in kinematic and dynamically consistent flows. *J. Atmos. Sci.,* **64,** 3640–3651, doi:10.1175/JAS4030.1.

Hegglin, M. I., and T. G. Shepherd, 2009: Large climate-induced changes in ultraviolet index and stratosphere-to-troposphere ozone flux. *Nat. Geosci.,* **2,** 687–691, doi:10.1038/ngeo604.

Holton, J. R., 1986: Meridional distribution of stratospheric trace constituents. *J. Atmos. Sci.,* **43,** 1238–1242, doi:10.1175/1520-0469(1986)043<1238:MDOSTC>2.0.CO;2.

——, P. H. Haynes, M. E. Mcintyre, A. R. Douglass, R. B. Rood, and L. Pfister, 1995: Stratosphere–troposphere exchange. *Rev. Geophys.,* **33,** 403–439, doi:10.1029/95RG02097.

Kerr-Munslow, A. M., and W. A. Norton, 2006: Tropical wave driving of the annual cycle in tropical tropopause temperatures. Part I: ECMWF analyses. *J. Atmos. Sci.,* **63,** 1410–1419, doi:10.1175/JAS3697.1.

Li, F., J. Austin, and J. Wilson, 2008: The strength of the Brewer–Dobson circulation in a changing climate: Coupled chemistry–climate model simulations. *J. Climate,* **21,** 40–57, doi:10.1175/2007JCLI1663.1.

Liu, J., and T. Schneider, 2011: Convective generation of equatorial superrotation in planetary atmospheres. *J. Atmos. Sci.,* **68,** 2742–2756, doi:10.1175/JAS-D-10-05013.1.

Lu, J., G. Chen, and D. M. W. Frierson, 2008: Response of the zonal mean atmospheric circulation to El Niño versus global warming. *J. Climate,* **21,** 5835–5851, doi:10.1175/2008JCLI2200.1.

Mahlman, J. D., H. I. Levy, and W. J. Moxim, 1986: Three-dimensional simulations of stratospheric N_2O: Predictions for other. *J. Geophys. Res.,* **91,** 2687–2707, doi:10.1029/JD091iD02p02687.

Matsuno, T., 1970: Vertical propagation of stationary planetary waves in the winter Northern Hemisphere. *J. Atmos. Sci.,* **27,** 871–883, doi:10.1175/1520-0469(1970)027<0871:VPOSPW>2.0.CO;2.

McLandress, C., and T. G. Shepherd, 2009: Simulated anthropogenic changes in the Brewer–Dobson circulation, including its extension to high latitudes. *J. Climate,* **22,** 1516–1540, doi:10.1175/2008JCLI2679.1.

Nakamura, N., 1996: Two-dimensional mixing, edge formation, and permeability diagnosed in an area coordinate. *J. Atmos. Sci.,* **53,** 1524–1537, doi:10.1175/1520-0469(1996)053<1524:TDMEFA>2.0.CO;2.

Neale, R. B., and B. J. Hoskins, 2000: A standard test for AGCMs including their physical parametrizations: I: The proposal. *Atmos. Sci. Lett.,* **1,** 101–107, doi:10.1006/asle.2000.0022.

Norton, W. A., 2006: Tropical wave driving of the annual cycle in tropical tropopause temperatures. Part II: Model results. *J. Atmos. Sci.,* **63,** 1420–1431, doi:10.1175/JAS3698.1.

Olsen, M. A., M. R. Schoeberl, and J. E. Nielsen, 2007: Response of stratospheric circulation and stratosphere–troposphere exchange to changing sea surface temperatures. *J. Geophys. Res.,* **112,** D16104, doi:10.1029/2006JD008012.

Plumb, R. A., 2002: Stratospheric transport. *J. Meteor. Soc. Japan,* **80,** 793–809.

Polvani, L., and P. Kushner, 2002: Tropospheric response to stratospheric perturbations in a relatively simple general circulation model. *Geophys. Res. Lett.,* **29,** 40–43, doi:10.1029/2001GL014284.

Randel, W. J., R. R. Garcia, and F. Wu, 2008: Dynamical balances and tropical stratospheric upwelling. *J. Atmos. Sci.,* **65,** 3584–3595, doi:10.1175/2008JAS2756.1.

——, ——, N. Calvo, and D. Marsh, 2009: ENSO influence on zonal mean temperature and ozone in the tropical lower stratosphere. *Geophys. Res. Lett.,* **36,** L15822, doi:10.1029/2009GL039343.

Ray, E. A., and Coauthors, 2010: Evidence for changes in stratospheric transport and mixing over the past three decades based on multiple data sets and tropical leaky pipe analysis. *J. Geophys. Res.,* **115,** D21304, doi:10.1029/2010JD014206.

Rind, D., D. Shindell, P. Lonergan, and N. K. Balachandran, 1998: Climate change and the middle atmosphere. Part III: The doubled CO_2 climate revisited. *J. Climate,* **11,** 876–894, doi:10.1175/1520-0442(1998)011<0876:CCATMA>2.0.CO;2.

Ryu, J.-H., and S. Lee, 2010: Effect of tropical waves on the tropical tropopause transition layer upwelling. *J. Atmos. Sci.,* **67,** 3130–3148, doi:10.1175/2010JAS3434.1.

Scinocca, J., and P. Haynes, 1998: Dynamical forcing of stratospheric planetary waves by tropospheric baroclinic eddies. *J. Atmos. Sci.,* **55,** 2361–2392, doi:10.1175/1520-0469(1998)055<2361:DFOSPW>2.0.CO;2.

Scott, R. K., and J. Cammas, 2002: Wave breaking and mixing at the subtropical tropopause. *J. Atmos. Sci.,* **59,** 2347–2361, doi:10.1175/1520-0469(2002)059<2347:WBAMAT>2.0.CO;2.

——, E. F. Shuckburgh, J. P. Cammas, and B. Legras, 2003: Stretching rates and equivalent length near the tropopause. *J. Geophys. Res.,* **108,** 4394, doi:10.1029/2002JD002988.

Shepherd, T. G., and C. McLandress, 2011: A robust mechanism for strengthening of the Brewer–Dobson circulation in response to climate change: Critical-layer control of subtropical wave breaking. *J. Atmos. Sci.,* **68,** 784–797, doi:10.1175/2010JAS3608.1.

Shuckburgh, E., F. D. Ovidio, and B. Legras, 2009: Local mixing events in the upper troposphere and lower stratosphere. Part II: Seasonal and interannual variability. *J. Atmos. Sci.,* **66,** 3695–3706, doi:10.1175/2009JAS2983.1.

Simpson, I. R., T. G. Shepherd, and M. Sigmond, 2011: Dynamics of the lower stratospheric circulation response to ENSO. *J. Atmos. Sci.,* **68,** 2537–2556, doi:10.1175/JAS-D-11-05.1.

Thompson, D. W. J., and S. Solomon, 2005: Recent stratospheric climate trends as evidenced in radiosonde data: Global structure and tropospheric linkages. *J. Climate,* **18,** 4785–4795, doi:10.1175/JCLI3585.1.

Waugh, D., 2009: Atmospheric dynamics: The age of stratospheric air. *Nat. Geosci.,* **2,** 14–16, doi:10.1038/ngeo397.

——, and T. Hall, 2002: Age of stratospheric air: Theory, observations, and models. *Rev. Geophys.,* **40,** 1010, doi:10.1029/2000RG000101.

Yang, H., K. Tung, and E. Olaguer, 1990: Nongeostrophic theory of zonally averaged circulation. Part II: Eliassen–Palm flux divergence and isentropic mixing coefficient. *J. Atmos. Sci.,* **47,** 215–241, doi:10.1175/1520-0469(1990)047<0215:NTOZAC>2.0.CO;2.